A Static Reduced-Order Multiple-Model Adaptive Estimator for Noise Identification

JOE KHALIFE, Member, IEEE
University of California, Irvine, CA USA

ZAHER M. KASSAS, Senior Member, IEEE
The Ohio State University, Columbus, OH USA

A reduced-order multiple-model (MM) estimator for noise identification in dynamic stochastic systems is developed. The unknown noise statistics are assumed to be static. While a standard static MM estimator does not grow exponentially over time, its computational complexity grows exponentially with the number of modes. The proposed algorithm reduces the computational complexity of MM estimation from exponential to polynomial by constructing a significantly smaller set of mode models, which are updated every time step. It is assumed that the constructed mode models do not change significantly between time steps, which in turn holds if the smoothness of the mode probabilities is guaranteed. It is shown that in the case where there is "enough" statistical distinction between the noise modes, the proposed reduced-order MM estimator converges to the standard MM estimator. The proposed reduced-order MM estimator is evaluated using Monte Carlo simulations, showing that it performs nearly similar to the standard MM estimator with a fraction of its complexity. The numerical example shows less than a 2% increase in the root mean-squared errors of the reduced-order MM estimator from the standard one, while the reduction in the number of filters in the reduced-order MM estimator is 300%. To further validate the proposed filter, experimental results are presented of an unmanned aerial vehicle (UAV) navigating with terrestrial signals of opportunity. Opportunistic navigation serves a relevant application for MM-based estimation, as system parameters, namely the statistics of the clock error dynamics of opportunistic sources, are unknown and must be adaptively estimated. The experimental results show a UAV navigating for more than 5 min over a trajectory of more than 3 km, achieving a final position error of 6.21 m obtained using the standard MM estimator versus a final position error of 6.25 m obtained using the proposed reduced-order MM estimator. A standard extended Kalman filter was implemented for comparative analysis, showing a final error of 40.03 m. In the experiments, the reduced-order MM estimator was implemented with 16 filters, while the standard MM was implemented with 256 filters.

Manuscript received 1 December 2021; revised 25 March 2022, 29 June 2022, and 13 October 2022; accepted 22 October 2022. Date of publication 6 January 2023; date of current version 9 June 2023.

DOI. No. 10.1109/TAES.2023.3234523

Refereeing of this contribution was handled by Y. Wu.

This work was supported in part by the Air Force Office of Scientific Research (AFOSR) under Grant FA9550-22-1-0476 and in part by the National Science Foundation (NSF) under Grant 2240512.

Authors' addresses: Joe Khalife was with the Department of Mechanical and Aerospace Engineering, University of California, Irvine, CA 92697 USA, E-mail: (jjkhalife@gmail.com); Zaher M. Kassas is with the Department of Electrical and Computer Engineering, The Ohio State University, Columbus, OH 43210 USA, E-mail: (zkassas@ieee.org). *(Corresponding author: Zaher M. Kassas.)*

I. INTRODUCTION

The ability to adaptively estimate unknown or poorly modeled system parameters is of particular interest in the ever advancing level of autonomy of ground, aerial, and space vehicles. Consider a self-driving car or an unmanned aerial vehicle (UAV) entering a poorly modeled, dynamic stochastic environment, such as an urban intersection [1], [2] or a signal landscape [3], [4]. As the vehicle navigates its environment, it must estimate its own states simultaneously with the environment's states, while refining its models of the surrounding environment.

Adaptive estimation approaches [5] can be categorized into Bayesian [6], [7], [8], covariance matching [9], [10], [11], correlation [12], [13], [14], maximum likelihood (ML) [15], [16], [17], and hybrid methods. A popular Bayesian technique is the multiple-model (MM) estimator. However, such estimators suffer from the curse of dimensionality in the presence of mode-switching [18], [19]. Covariance matching techniques rely on the principle of making the time average of squared innovations consistent with the ensemble average; hence, they implicitly assume ergodicity of the noise. Tuning the process noise covariance is typically done in an ad hoc manner, making the convergence of these techniques questionable [20], [21]. Correlation methods assume ergodicity of the noise and rely on establishing relationships between the noise statistics and the autocorrelation of the measurement or residual sequences. They have been shown to be a fruitful approach [22], [23], [24]. In ML techniques, the likelihood function is maximized to obtain estimates of the noise statistics, and the chain rule of probability distributions is typically invoked. A unique solution is only guaranteed whenever the dimension of the observation vector is greater than or equal to the dimension of the state vector [25], [26]. The most popular hybrid techniques are the MM adaptive estimator with mode switching [27], [28] and the interacting multiple-model (IMM) estimator [29], [30]. MM estimation has been used in a variety of applications, ranging from positioning and navigation [31], [32], target tracking [33], [34], air traffic control [35], [36], fault detection [37], [38], cognitive radio [39], [40], and many more. MM estimators have been "adapted" to estimating process and measurement noise statistics [41].

Both MM and IMM estimators maintain a bank of Kalman filters (KFs) matched to the various modes at which the system may be operating. The innovation likelihoods from each filter are used to weight the filter estimates

to form a combined state estimate. The standard static MM adaptive estimator directly uses these likelihoods as adaptive weights, which could cause the filter to converge onto a particular mode. To rectify this behavior, minimum threshold probabilities are typically assigned to each filter. The IMM circumvents this problem with the introduction of an interaction/mixing step in which state estimates given to the bank of filters are calculated at each time step using the weighted estimates of the previous time step. While the IMM and its derivatives reduce the computational complexity as a function of time, the literature falls short on addressing the computational complexity of MM-based estimator as a function of the number of possible modes.

This article considers the following problem. A stochastic linear time-varying (LTV) system with N process noise elements, each of which can be in M modes. As such, a full implementation of standard MM estimators requires M^N filters to exhaust all possible modes. This exploding complexity renders MM estimators impractical for moderately large-scale systems. This article aims to develop a reduced-order MM estimator that only requires $M \cdot N$ filters. A particular application that would benefit from such reduction in complexity is navigation with signals of opportunity (SOPs), which are ambient signals not intended for navigation purposes [42]. SOPs have been demonstrated to be a promising complement or alternative to global navigation satellite system (GNSS) signals in GNSS-challenged environments [43], [44]. Examples of SOPs include AM/FM radio [45], [46], digital television [47], [48], cellular [49], [50], [51], [52], and low Earth orbit (LEO) satellites [53], [54], [55], [56]. Cellular signals proved to be particularly attractive due to their spatial and spectral diversity, high received power, and cost-free usage of their downlink synchronization signals. Cellular SOP receivers were designed to extract navigation observables from such signals [57], [58], [59], [60], [61], e.g., pseudorange and carrier phase measurements. Both the pseudorange and carrier phase measurements give a measure of the range between the transmitter and receiver up to some bias due to the difference between the transmitter's and receiver's clocks. The cellular SOP transmitters, known as base transceiver stations (BTSs), may be asynchronous and have unknown clock biases, which are dynamic and stochastic processes. When the statistics of these processes are unknown to the estimator, the filter will be mismatched to the true model, which in turn would degrade the estimation performance and more dangerously, could cause filter divergence altogether. One way to circumvent this mismatch is to use an adaptive MM estimator, where each estimator is matched to the statistics of some possible clock oscillator quality. A preliminary study demonstrated the efficacy of this approach, where two modes per transmitter were employed, one pertaining to a low quality oscillator and one to a high quality oscillator, and the mode probability was used as a weight [62].

The number of estimators needed for a standard MM estimator grows exponentially with the number of transmitters, especially in the case of aerial vehicle navigation, where the number of visible transmitters increases due to favorable radio propagation channels [63]. Assuming two possible models per transmitter clock, employing a standard MM estimator, $2^8 = 1024$ filters would be needed for eight transmitters. As the number of transmitters increases even further; which could easily happen with LEO SOPs [64], [65], where hundreds of LEO satellites could be simultaneously visible [4]; the computational complexity of MM estimators becomes practically infeasible to implement on small UAVs with limited computational power.

Motivated by the need of a computationally efficient MM estimator, the contributions of this article are as follows.

1) A reduced-order MM estimator is proposed to adaptively estimate the process and measurement noise covariance in stochastic LTV systems. The proposed algorithm performs nearly similar to a standard MM estimator with a fraction of the computational complexity.
2) A sufficient condition for the reduced-order MM estimator to converge to a standard estimator is derived.
3) Monte Carlo simulations are presented to evaluate the proposed algorithm, showing a less than 2% difference in the root mean-squared error (RMSE) of the proposed algorithm compared to the standard MM estimator.
4) Experimental results are presented, showing a UAV navigating for more than 5 min over a trajectory of more than 3 km with the proposed algorithm. The reduced-order MM estimator is compared with a standard MM estimator and a standard extended Kalman filter (EKF). A final position error of 6.21 m is obtained using the standard MM estimator implemented with 256 filters while a final position error of 6.25 m is obtained using the proposed reduced-order MM estimator implemented with 16 filters only.

The rest of this article is organized as follows. Section II provides the system model and gives an overview of standard MM estimation. Section III describes the reduced-order MM algorithm. Section IV presents simulation results. Section V presents experimental results. Finally, Section VI concludes this article.

II. SYSTEM MODEL AND MM ESTIMATION OVERVIEW

This section presents the models adopted in this article and gives an overview of MM estimators.

A. System Model

Consider the following discrete-time LTV system

$$\boldsymbol{x}(k+1) = \mathbf{F}(k)\boldsymbol{x}(k) + \boldsymbol{w}(k) \tag{1}$$

$$\boldsymbol{z}(k) = \mathbf{H}(k)\boldsymbol{x}(k) + \boldsymbol{v}(k), \quad k = 0, 1, \ldots \tag{2}$$

where $\boldsymbol{x}(k) \in \mathbb{R}^{n_x}$ is the state vector; $\mathbf{F}(k)$ is the state transition matrix; $\boldsymbol{z}(k) \in \mathbb{R}^{n_z}$ is the measurement vector; $\mathbf{H}(k)$ is the output matrix; and $\boldsymbol{w}(k)$ and $\boldsymbol{v}(k)$ are zero-mean white Gaussian random sequences with covariances $\mathbf{Q}(k)$ and

$\mathbf{R}(k)$, respectively. Let Z^k denote the set of all measurements up to time k, i.e., $Z^k \triangleq \{z(\kappa)\}_{\kappa=0}^{k}$. The time index k will be subsequently dropped for compactness of notation, unless explicitly specified. Consider the process noise vector $\boldsymbol{w} = [w_1, w_2, \ldots, w_{n_x}]^{\mathsf{T}}$. Each w_l can be in one of r_l modes, where each particular mode has a corresponding variance σ_l^2 and cross-covariance $\sigma_{ll'}$ for $l' \in \{1, \ldots, n_x\}\backslash l$. Let L denote the total number of process noise elements for which $r_l > 1$. The resulting process noise covariance can always be expressed as a linear combination of these L elements as given by

$$\mathbf{Q} = \sum_{l=1}^{L} \boldsymbol{\Gamma}_l \mathbf{Q}^l \boldsymbol{\Gamma}_l^{\mathsf{T}} \tag{3}$$

where $\boldsymbol{\Gamma}_l$ are known constant matrices and $\mathbf{Q}^l \in \{\mathbf{Q}_i^l\}_{i=1}^{r_l}$, and r_l is number of possible "modes" of process noise element l. In this article, it is assumed that all elements of the process noise covariance matrix are in a fixed but unknown mode $\forall\ k \geq 0$, i.e.,

$$\mathbf{Q}^l = \mathbf{Q}_{n_l}^l \qquad \forall\ k \geq 0 \tag{4}$$

where n_l is the active mode of the lth element. To illustrate (3) and (4), consider a double integrator system driven by process noise. This system is typically used to model the behavior of crystal oscillator clocks, a crucial element in radionavigation. The discrete-time process noise covariance of these models is expressed as

$$\mathbf{Q} = \begin{bmatrix} S_1 T + S_2 \frac{T^3}{3} & S_2 \frac{T^2}{2} \\ S_2 \frac{T^2}{2} & S_2 T \end{bmatrix} \tag{5}$$

where T is the sampling time and S_1 and S_2 are the continuous-time power spectra of the clock bias and drift. The quantities S_1 and S_2 vary with the quality of the oscillator. When these quantities are unknown, one can use an MM estimator to estimate them along with the clock states. It is assumed that S_1 and S_2 are given from the sets $\mathcal{S}_1$ and $\mathcal{S}_2$, respectively. A standard MM estimator would require a number of filters that is equal to the product of the cardinalities of $\mathcal{S}_1$ and $\mathcal{S}_2$. The goal of the reduced-order MM is to adaptively estimate S_1 and S_2 with lower complexity. As such, one can rewrite the process noise covariance in (5) as

$$\mathbf{Q} = \sum_{l=1}^{2} \boldsymbol{\Gamma}_l \mathbf{Q}^l \boldsymbol{\Gamma}_l^{\mathsf{T}} \tag{6}$$

where

$$\mathbf{Q}^1 = S_1 T, \quad \mathbf{Q}^2 = \begin{bmatrix} S_2 \frac{T^3}{3} & S_2 \frac{T^2}{2} \\ S_2 \frac{T^2}{2} & S_2 T \end{bmatrix}, \quad \boldsymbol{\Gamma}_1 = [1, 0]^{\mathsf{T}}, \quad \boldsymbol{\Gamma}_2 = \mathbf{I}_{2\times 2} \tag{7}$$

and $\mathbf{I}_{n\times n}$ is the $n \times n$ identity matrix. Note that $\boldsymbol{\Gamma}_1$ and $\boldsymbol{\Gamma}_2$ are constant and known matrices. The quantity $\mathbf{Q}^1$ is solely dependent on S_1, which is unknown but is given from the set $\mathcal{S}_1$ and $\mathbf{Q}^2$ is solely dependent on S_2, which is also unknown but is given from the set $\mathcal{S}_2$. As will be shown in the following section, expressing $\mathbf{Q}$ as in (3) will be crucial in the formulation of the reduced-order MM estimator, as it allows us to estimate the process noise covariance of each element separately from the rest, reducing the number of filters needed to the sum of cardinalities of $\mathcal{S}_1$ and $\mathcal{S}_2$ instead of their product.

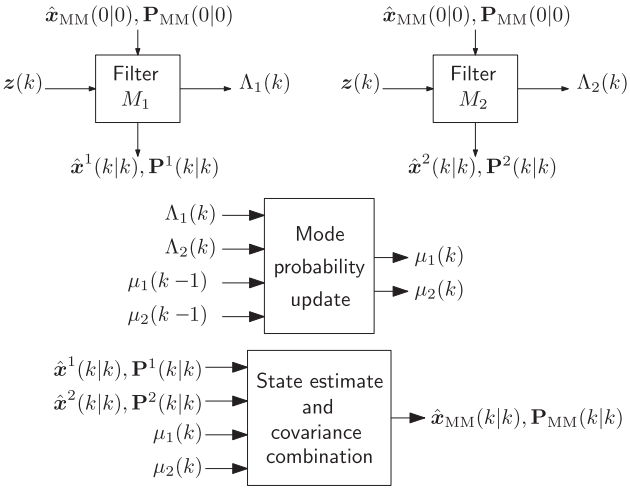

Fig. 1. Standard MM estimator for $r = 2$ fixed models.

Similarly to the process noise covariance, the measurement noise covariance can generally be expressed as a linear combination of J elements as given by

$$\mathbf{R} = \sum_{j=1}^{J} \boldsymbol{\Psi}_j \mathbf{R}^j \boldsymbol{\Psi}_j^{\mathsf{T}} \tag{8}$$

where $\boldsymbol{\Psi}_j$ are known constant matrices and $\mathbf{R}^j \in \{\mathbf{R}_i^j\}_{i=1}^{s_j}$, and s_j is number of possible modes of measurement noise element j. Moreover, it is assumed that all elements of the measurement noise covariance matrix are in a fixed but unknown mode $\forall\ k \geq 0$, i.e.,

$$\mathbf{R}^j = \mathbf{R}_{o_j}^j \qquad \forall\ k \geq 0 \tag{9}$$

where o_j is the active mode of the jth element. Note that it is assumed that $\mathbf{Q} \succ 0$ and $\mathbf{R} \succ 0$.

B. Overview of the Standard MM Estimator

In MM estimation, the system is assumed to obey one of a finite number of modes, and a bank of estimators (usually KFs) run in parallel, where each filter is matched to a particular mode. A state estimate is computed by summing the individual filter estimates, weighted by their respective innovation likelihoods [66].

1) *Simple MM Estimator Formulation:* A single cycle of the standard MM estimator for $r = 2$ models is depicted in Fig. 1, with the following notational definitions:

r	Number of filters.
i	$\{1, \ldots, r\} \in \mathbb{N}$.
M_i	Hypothesis that mode i is active.
$\hat{\boldsymbol{x}}^i(k\|k)$	State estimate of filter i.
$\mathbf{P}^i(k\|k)$	Estimation error covariance of filter i.
$\Lambda_i(k+1)$	Innovation likelihood of filter i.
$\hat{\boldsymbol{x}}^i(k+1\|k+1)$	Updated state estimate of filter i.

$\mathbf{P}^i(k+1\|k+1)$	Updated estimation error covariance of filter i.
$\mu_i(k+1)$	Mode probability of filter i.
$\hat{\boldsymbol{x}}_{\mathrm{MM}}(k+1\|k+1)$	Combined state estimate in the MM estimator.
$\mathbf{P}_{\mathrm{MM}}(k+1\|k+1)$	Combined estimation error covariance in the MM estimator.

The MM estimator consists of the following three stages: filtering, mode probability update, and combination, which are summarized as follows.

1) *Mode-matched filtering:* These stages perform a regular KF update (prediction and correction), for each KF in the bank, where each filter is matched to a particular mode to produce estimates $\hat{\boldsymbol{x}}^i(k+1|k+1)$ and associated estimation error covariance $\mathbf{P}^i(k+1|k+1)$. It also calculates the innovation likelihood functions according to

$$\Lambda_i(k+1) = \mathcal{N}\left[\boldsymbol{v}^i(k+1); \mathbf{0}, \mathbf{S}^i(k+1)\right] \tag{10}$$

where $\mathcal{N}[\boldsymbol{x}; \boldsymbol{\mu}, \boldsymbol{\Sigma}]$ denotes the multivariate Gaussian probability density function with mean vector $\boldsymbol{\mu}$ and covariance matrix $\boldsymbol{\Sigma}$ evaluated at some vector $\boldsymbol{x}$, $\boldsymbol{v}^i(k+1)$ is the innovation vector in filter i, and $\mathbf{S}^i(k+1)$ is the innovation covariance in filter i.

2) *Mode probability update:* This stage updates the mode probabilities based on the innovation likelihoods using Bayes' formula, which can be shown to be

$$\mu_i(k+1) = \frac{\Lambda_i(k+1)\mu_i(k)}{\sum_{j=1}^{k} \Lambda_j(k+1)\mu_j(k)}. \tag{11}$$

3) *State estimate and covariance combination:* This stage combines the state estimates and estimation error covariances from the individual filters by weighting $\hat{\boldsymbol{x}}^i(k+1|k+1)$ and $\mathbf{P}^i(k+1|k+1)$ by their respective mode probabilities $\mu_i(k+1)$ according to

$$\hat{\boldsymbol{x}}_{\mathrm{MM}}(k+1|k+1) = \sum_{j=1}^{r} \mu_j(k+1)\hat{\boldsymbol{x}}^j(k+1|k+1) \tag{12}$$

$$\begin{aligned}\mathbf{P}_{\mathrm{MM}}(k+1|k+1) = \sum_{j=1}^{r} \mu_j(k+1) \Big\{ & \mathbf{P}^j(k+1|k+1) \\ & + \left[\hat{\boldsymbol{x}}^j(k+1|k+1) - \hat{\boldsymbol{x}}_{\mathrm{MM}}(k+1|k+1)\right] \\ & \cdot \left[\hat{\boldsymbol{x}}^j(k+1|k+1) - \hat{\boldsymbol{x}}_{\mathrm{MM}}(k+1|k+1)\right]^{\mathrm{T}} \Big\}.\end{aligned} \tag{13}$$

After some time, the mode probability of the active mode in the MM estimator will converge to unity and the others to zero. After convergence, the estimate and estimation error covariance will converge to those of a KF matched to the true active mode. Let $\hat{\boldsymbol{x}}(k|k)$ and $\mathbf{P}(k|k)$ denote the matched estimate and estimation error covariance. As such, after convergence, the following holds: $\hat{\boldsymbol{x}}_{\mathrm{MM}}(k|k) = \hat{\boldsymbol{x}}(k|k)$ and $\mathbf{P}_{\mathrm{MM}}(k|k) = \mathbf{P}(k|k)$.

2) *MM Estimator Formulation for the System in (1) and (2):* Let $M_{i_l}^l$ denote the event that the i_lth mode of the lth process noise element is active and $N_{t_j}^j$ the fact that the t_jth mode of the jth measurement noise element is active. Next, let $\mu_{i_1,\ldots,i_L,t_1,\ldots,t_J}(k)$ denote the probability that $\{M_{i_1}^1, \ldots, M_{i_L}^L, N_{t_1}^1, \ldots, N_{t_J}^J\}$ are active given Z^k, hence

$$\mu_{i_1,\ldots,i_L,t_1,\ldots,t_J}(k) = \Pr\left[M_{i_1}^1, \ldots, M_{i_L}^L, N_{t_1}^1, \ldots, N_{t_J}^J \,|\, Z^k\right]. \tag{14}$$

In the standard MM approach, it is assumed that there is a filter matched for each combination $\{M_{i_1}^1, \ldots, M_{i_L}^L, N_{t_1}^1, \ldots, N_{t_J}^J\}$. Let $\hat{\boldsymbol{x}}_{i_1,\ldots,i_L,t_1,\ldots,t_J}(k|k)$ denote the current estimate in the filter matched to $\{M_{i_1}^1, \ldots, M_{i_L}^L, N_{t_1}^1, \ldots, N_{t_J}^J\}$ and $\mathbf{P}_{i_1,\ldots,i_L,t_1,\ldots,t_J}(k|k)$ its corresponding estimation error covariance. Similarly to (12), the combined estimate in this case will be given by

$$\begin{aligned}\hat{\boldsymbol{x}}_{\mathrm{MM}}(k|k) = & \sum_{i_1} \cdots \sum_{i_L} \sum_{t_1} \cdots \sum_{t_J} \mu_{i_1,\ldots,i_L,t_1,\ldots,t_J}(k) \\ & \cdot \hat{\boldsymbol{x}}_{i_1,\ldots,i_L,t_1,\ldots,t_J}(k|k)\end{aligned} \tag{15}$$

with the estimation error covariance

$$\begin{aligned}\mathbf{P}_{\mathrm{MM}}(k|k) = & \sum_{i_1} \cdots \sum_{i_L} \sum_{t_1} \cdots \sum_{t_J} \mu_{i_1,\ldots,i_L,t_1,\ldots,t_J}(k) \\ & \cdot \Big\{ \mathbf{P}_{i_1,\ldots,i_L,t_1,\ldots,t_J}(k|k) \\ & + \left[\hat{\boldsymbol{x}}_{i_1,\ldots,i_L,t_1,\ldots,t_J}(k|k) - \hat{\boldsymbol{x}}_{\mathrm{MM}}(k|k)\right] \\ & \cdot \left[\hat{\boldsymbol{x}}_{i_1,\ldots,i_L,t_1,\ldots,t_J}(k|k) - \hat{\boldsymbol{x}}_{\mathrm{MM}}(k|k)\right]^{\mathrm{T}} \Big\}.\end{aligned} \tag{16}$$

Consequently, in order to run an MM estimator for the system defined in (1) and (2), the number of filters needed is given by

$$N_{\mathrm{filters}} = \prod_{l=1}^{L} r_l \prod_{j=1}^{J} s_j. \tag{17}$$

Assuming $r_1 = r_2 = \cdots = r_L = r$ and $s_1 = s_2 = \cdots = s_J = s$, then $N_{\mathrm{filters}} = r^L s^J$, which grows exponentially with the number of elements L and J. The following section proposes a near-optimal MM-based estimator where the number of required filters does not scale exponentially.

III. REDUCED-ORDER MM ESTIMATOR

The reduced-order MM estimator is developed in the following equation.

A. Motivation of the Reduced-Order MM Estimator

MM estimators were also used to estimate the unknown process noise statistics in [41], where a bank of two KFs are identically initialized with the exception of $\mathbf{Q}^i$. One of the filters was initialized with an upper-bound $\mathbf{Q}_{\max}$, while the other is initialized with a lower-bound $\mathbf{Q}_{\min}$, corresponding to the worst and best case process noise scenarios. In this scheme, the noise covariance estimate $\hat{\mathbf{Q}}$ is computed as

$$\hat{\mathbf{Q}}(k) = \sum_{i=1}^{2} \mu_i(k)\, \mathbf{Q}^i(k). \tag{18}$$

This can be similarly done for the measurement covariance as

$$\hat{\mathbf{R}}(k) = \sum_{i=1}^{2} \mu_i(k)\, \mathbf{R}^i(k). \tag{19}$$

This can be generalized for the case of an MM estimator for system (1) and (2), where

$$\begin{aligned}\hat{\mathbf{Q}}(k) =& \sum_{i_1} \cdots \sum_{i_L} \sum_{t_1} \cdots \sum_{t_J} \mu_{i_1,\ldots,i_L,t_1,\ldots,t_J}(k) \sum_{l=1}^{L} \boldsymbol{\Gamma}_l \mathbf{Q}_{i_l}^l \boldsymbol{\Gamma}_l^{\mathrm{T}} \\ =& \sum_{l=1}^{L} \sum_{i_1} \cdots \sum_{i_L} \boldsymbol{\Gamma}_l \mathbf{Q}_{i_l}^l \boldsymbol{\Gamma}_l^{\mathrm{T}} \sum_{t_1} \cdots \sum_{t_J} \mu_{i_1,\ldots,i_L,t_1,\ldots,t_J}(k)\end{aligned} \tag{20}$$

and

$$\begin{aligned}\hat{\mathbf{R}}(k) =& \sum_{i_1} \cdots \sum_{i_L} \sum_{t_1} \cdots \sum_{t_J} \mu_{i_1,\ldots,i_L,t_1,\ldots,t_J}(k) \sum_{j=1}^{J} \boldsymbol{\Psi}_j \mathbf{R}_{t_j}^j \boldsymbol{\Psi}_j^{\mathrm{T}} \\ =& \sum_{j=1}^{J} \sum_{t_1} \cdots \sum_{t_J} \boldsymbol{\Psi}_l \mathbf{R}_{l_j}^j \boldsymbol{\Psi}_j^{\mathrm{T}} \sum_{i_1} \cdots \sum_{i_L} \mu_{i_1,\ldots,i_L,t_1,\ldots,t_J}(k).\end{aligned} \tag{21}$$

The following lemma motivates the main idea behind the reduced-order MM estimator.

LEMMA III.1 Consider an MM estimator for the system in (1) and (2). Then, the process noise and measurement noise covariance estimates may be expressed as

$$\hat{\mathbf{Q}}(k) = \frac{1}{L} \sum_{l=1}^{L} \sum_{i_l} \mu_{i_l}^{q,l}(k) \bar{\mathbf{Q}}_{i_l}^l(k) \tag{22}$$

$$\hat{\mathbf{R}}(k) = \frac{1}{J} \sum_{j=1}^{J} \sum_{t_j} \mu_{t_j}^{r,j}(k) \bar{\mathbf{R}}_{t_j}^j(k) \tag{23}$$

where $\mu_{i_l}^{q,l}(k)$ and $\mu_{t_j}^{r,j}(k)$ are some appropriately defined probabilities, i.e., $\sum \mu_{i_l}^{q,l}(k) = 1$ and $\sum \mu_{t_j}^{r,j}(k) = 1$, and

$$\bar{\mathbf{Q}}_{i_m}^m(k) \triangleq \boldsymbol{\Gamma}_m \mathbf{Q}_{i_m}^m \boldsymbol{\Gamma}_m^{\mathrm{T}} + \bar{\mathbf{Q}}^m(k) \tag{24}$$

$$\bar{\mathbf{R}}_{i_p}^p(k) \triangleq \boldsymbol{\Psi}_p \mathbf{R}_{t_p}^p \boldsymbol{\Psi}_p^{\mathrm{T}} + \bar{\mathbf{R}}^p(k) \tag{25}$$

where

$$\bar{\mathbf{Q}}^m(k) \triangleq \sum_{\substack{l=1 \\ l \neq m}}^{L} \sum_{i_l} \mu_{i_l}^{q,l}(k) \boldsymbol{\Gamma}_l \mathbf{Q}_{i_l}^l \boldsymbol{\Gamma}_l^{\mathrm{T}} \tag{26}$$

$$\bar{\mathbf{R}}^p(k) \triangleq \sum_{\substack{j=1 \\ j \neq p}}^{J} \sum_{t_j} \mu_{t_j}^{r,j}(k) \boldsymbol{\Psi}_j \mathbf{R}_{t_j}^j \boldsymbol{\Psi}_j^{\mathrm{T}}. \tag{27}$$

PROOF See the Appendix.

Lemma III.1 implies that the estimated process and measurement noise covariances can be expressed as a sum of $\sum_{l=1}^{L} r_l$ and $\sum_{j=1}^{J} s_j$ terms, respectively. For simplicity, assume $J = 1$ with $s_1 = s = 1$ and $r_l = r$. Then, (22) can be interpreted as the estimated process noise covariance from L banks of filters, each bank with r sub-banks of filters, with each particular filter matched to the process noise covariance given in (24). A similar interpretation can be made for $\hat{\mathbf{R}}(k)$ in the general case. Consequently, when all L and J banks of filters converge, i.e., the mode probabilities $\mu_{i_l}^{q,l}(k)$ and $\mu_{t_j}^{r,j}(k)$ become

$$\mu_{i_l}^{q,l}(k) = \mu_{i_l}^{q,l} = \begin{cases} 1, & \text{if } i_l = n_l, \\ 0, & \text{otherwise} \end{cases} \quad \forall\ l = 1, \ldots, L$$

and

$$\mu_{t_j}^{r,j}(k) = \mu_{tj}^{r,j} = \begin{cases} 1, & \text{if } t_j = o_j, \\ 0, & \text{otherwise} \end{cases} \quad \forall\ j = 1, \ldots, J$$

then it can be readily shown that $\bar{\mathbf{Q}}_{i_m}^m(k) = \mathbf{Q}(k)$ and $\bar{\mathbf{R}}_{i_p}^p(k) = \mathbf{R}(k)$, which in turn implies that $\hat{\mathbf{Q}}(k) = \mathbf{Q}(k)$ and $\hat{\mathbf{R}}(k) = \mathbf{R}(k)$. ■

B. Reduced-Order MM Algorithm

Motivated by the results of Lemma III.1, the reduced-order MM estimator algorithm is developed. The proposed algorithm requires a total of $U = \sum_{l=1}^{L} r_l + \sum_{j=1}^{J} s_j$ filters and operates similarly to the standard MM estimator with some differences highlighted in the following steps. Let $\hat{\mu}_{i_l}^{q,l}$ denote the mode probability of the filter matched to the i_lth mode of the lth process noise element and $\hat{\mu}_{t_j}^{r,j}$ denote the mode probability of the filter matched to the t_jth mode of the jth measurement noise element.

1) *Model Construction:* In this stage, a model for each mode-matched filter is constructed as follows. Let $u \in \{1, 2, \ldots, U\}$ denote the uth mode-matched filter. Note that if $u \leq \sum_{l=1}^{L} r_l$, then u can be mapped to an element m of the process noise. In this case, the uth process noise covariance, which is the one matched to the i_mth mode of the mth process noise element, is constructed as

$$\hat{\mathbf{Q}}^u(k) = \boldsymbol{\Gamma}_m \mathbf{Q}_{i_m}^m \boldsymbol{\Gamma}_m^{\mathrm{T}} + \hat{\bar{\mathbf{Q}}}^m(k) \tag{28}$$

where

$$\hat{\bar{\mathbf{Q}}}^m(k) = \sum_{\substack{l=1 \\ l \neq m}}^{L} \sum_{i_l} \hat{\mu}_{i_l}^{q,l}(k) \boldsymbol{\Gamma}_l \mathbf{Q}_{i_l}^l \boldsymbol{\Gamma}_l^{\mathrm{T}}. \tag{29}$$

The mode-matched measurement noise covariance will be given by

$$\hat{\mathbf{R}}^u(k) = \sum_{j=1}^{J} \sum_{t_j} \hat{\mu}_{t_j}^{r,j}(k) \boldsymbol{\Psi}_j \mathbf{R}_{t_j}^j \boldsymbol{\Psi}_j^{\mathrm{T}}. \tag{30}$$

Alternatively, if $u > \sum_{l=1}^{L} r_l$ then u can be mapped to the t_mth model of the mth measurement noise element. In this case, the mode-matched process noise covariance is constructed as

$$\hat{\mathbf{Q}}^u(k) = \sum_{l=1}^{L} \sum_{i_l} \hat{\mu}_{i_l}^{q,l}(k) \boldsymbol{\Gamma}_l \mathbf{Q}_{i_l}^l \boldsymbol{\Gamma}_l^{\mathrm{T}}. \tag{31}$$

The mode-matched measurement noise covariance will be given by

$$\hat{\mathbf{R}}^u(k) = \boldsymbol{\Psi}_m \mathbf{R}^m_{t_m} \boldsymbol{\Psi}^{\mathrm{T}}_m + \hat{\bar{\mathbf{R}}}^m(k) \tag{32}$$

where

$$\hat{\bar{\mathbf{R}}}^m(k) = \sum_{\substack{j=1 \\ j\neq m}}^{J} \sum_{t_j} \hat{\mu}^{r,j}_{t_j}(k) \boldsymbol{\Psi}_j \mathbf{R}^j_{t_j} \boldsymbol{\Psi}^{\mathrm{T}}_j. \tag{33}$$

2) *Mode-Matched Filtering:* After model construction, each filter is updated and the likelihood functions denoted by $\Lambda^l_{i_l}(k)$ and $\Lambda^j_{t_j}(k)$ are computed similarly to the MM estimator shown in (10). For details about mode-matched filtering and likelihood function calculations, the reader is referred to [66].

3) *Mode Probability Update:* Similar to the standard MM equations, the mode probabilities $\hat{\mu}^{q,l}_{i_l}$ and $\hat{\mu}^{r,j}_{t_j}$ are updated using $\Lambda^l_{i_l}(k)$ and $\Lambda^j_{t_j}(k)$ according to (11). This step assumes that the constructed models do not vary significantly between time steps. The assumption is discussed further in Section III-D.

4) *State Estimate and Covariance Combination:* Let $\hat{\boldsymbol{x}}'_{\mathrm{MM}}(k|k)$ and $\mathbf{P}'_{\mathrm{MM}}(k|k)$ denote the state estimate and covariance of the reduced-order MM estimator. Moreover, let $\hat{\boldsymbol{x}}^{q,l}_{i_l}(k|k)$ and $\mathbf{P}^{q,l}_{i_l}(k|k)$ denote the estimate and estimation error covariance maintained in the filter matched to the i_lth mode of the lth process noise element, and $\hat{\boldsymbol{x}}^{r,j}_{t_j}(k|k)$ and $\mathbf{P}^{r,j}_{t_j}(k|k)$ denote the estimate and estimation error covariance maintained in the filter matched to the t_jth mode of the jth measurement noise element. Subsequently, the state estimate and covariance combination is performed similarly to the standard MM estimator and is given by

$$\hat{\boldsymbol{x}}'_{\mathrm{MM}}(k|k) = \frac{1}{L+J}\left[\sum_{l=1}^{L}\sum_{i_l} \hat{\mu}^{q,l}_{i_l}(k)\hat{\boldsymbol{x}}^{q,l}_{i_l}(k|k) + \sum_{j=1}^{J}\sum_{t_j} \hat{\mu}^{r,j}_{t_j}(k)\hat{\boldsymbol{x}}^{r,j}_{t_j}(k|k)\right]. \tag{34}$$

The estimation error covariance is given by

$$\begin{aligned}\hat{\mathbf{P}}'_{\mathrm{MM}}(k|k) = \frac{1}{L+J}\Bigg\{&\sum_{l=1}^{L}\sum_{i_l} \hat{\mu}^{q,l}_{i_l}(k)\Big\{\mathbf{P}^{q,l}_{i_l}(k|k) \\ &+ \left[\hat{\boldsymbol{x}}^{q,l}_{i_l}(k|k) - \hat{\boldsymbol{x}}'_{\mathrm{MM}}(k|k)\right] \\ &\cdot \left[\hat{\boldsymbol{x}}^{q,l}_{i_l}(k|k) - \hat{\boldsymbol{x}}'_{\mathrm{MM}}(k|k)\right]^{\mathrm{T}}\Big\} \\ &+ \sum_{j=1}^{J}\sum_{t_j} \hat{\mu}^{r,j}_{t_j}(k)\Big\{\mathbf{P}^{r,j}_{t_j}(k|k) \\ &+ \left[\hat{\boldsymbol{x}}^{r,j}_{t_j}(k|k) - \hat{\boldsymbol{x}}'_{\mathrm{MM}}(k|k)\right] \\ &\cdot \left[\hat{\boldsymbol{x}}^{r,j}_{t_j}(k|k) - \hat{\boldsymbol{x}}'_{\mathrm{MM}}(k|k)\right]^{\mathrm{T}}\Big\}\Bigg\}.\end{aligned} \tag{35}$$

Note that similar to the standard MM estimator, the process noise and measurement noise covariances may be estimated as

$$\hat{\mathbf{Q}}(k) = \sum_{l=1}^{L}\sum_{i_l} \hat{\mu}^{l}_{i_l}(k)\boldsymbol{\Gamma}_l \mathbf{Q}^l_{i_l} \boldsymbol{\Gamma}^{\mathrm{T}}_l \tag{36}$$

$$\hat{\mathbf{R}}(k) = \sum_{j=1}^{J}\sum_{t_j} \hat{\mu}^{j}_{t_j}(k)\boldsymbol{\Psi}_j \mathbf{R}^j_{t_j} \boldsymbol{\Psi}^{\mathrm{T}}_j. \tag{37}$$

C. Optimality of the Reduced-Order MM Estimator

The reduced-order MM estimator comprises $L+J$ banks of filters, one for each process noise and measurement noise element. The lth bank of process noise elements contains a sub-bank of r_l filters, each matched to one of the r_l modes that the lth process noise element can be in. In other words, the lth bank is running r_l filters, each filter matched to a process noise covariance from the set $\{\bar{\mathbf{Q}}^l_{i_l}(k)\}^{r_l}_{i_l=1}$. Similarly, the jth bank of measurement noise elements contains a sub-bank of s_j filters, each matched to one of the s_j modes that the jth measurement noise element can be in. In other words, the jth bank is running s_j filters, each filter matched to a measurement noise covariance from the set $\{\bar{\mathbf{R}}^j_{t_j}(k)\}^{s_j}_{t_j=1}$. Recall that $\hat{\boldsymbol{x}}(k|k)$ and $\mathbf{P}(k|k)$ denote the estimate of $\boldsymbol{x}$ and its associated estimation error covariance in a KF matched to the true statistics $\mathbf{Q}$ and $\mathbf{R}$. As such, if the mode probabilities in the reduced-order MM converge to the right values, i.e.,

$$\hat{\mu}^{q,l}_{i_l}(k) = \hat{\mu}^{q,l}_{i_l} = \begin{cases}1, & \text{if } i_l = n_l, \\ 0, & \text{otherwise}\end{cases} \qquad \forall\ l = 1, \ldots, L \tag{38}$$

$$\hat{\mu}^{r,j}_{t_j}(k) = \hat{\mu}^{r,j}_{tj} = \begin{cases}1, & \text{if } t_j = o_j, \\ 0, & \text{otherwise}\end{cases} \qquad \forall\ j = 1, \ldots, J \tag{39}$$

then, it can be readily shown combining (36)–(39) that the estimated process and measurement noise covariances converge to the true ones, i.e.,

$$\hat{\mathbf{Q}}(k) \to \mathbf{Q}(k), \qquad \hat{\mathbf{R}}(k) \to \mathbf{R}(k). \tag{40}$$

As a result, the filters for which $\hat{\mu}^{q,l}_{i_l} = 1$ and $\hat{\mu}^{r,j}_{t_j} = 1$ will be matched to $\mathbf{Q}$ and $\mathbf{R}$, which in turn means that their state estimate and estimation error covariances will converge to $\hat{\boldsymbol{x}}(k|k)$ and $\mathbf{P}(k|k)$. As such, if (38) and (39) hold, then it follows that

$$\hat{\boldsymbol{x}}'_{\mathrm{MM}}(k|k) \to \hat{\boldsymbol{x}}(k|k), \qquad \hat{\mathbf{P}}'_{\mathrm{MM}}(k|k) \to \hat{\mathbf{P}}(k|k). \tag{41}$$

In other words, if (38) and (39) hold, then the reduced-order MM estimator converges to that of a matched KF, which is known to be the optimal estimator of $\boldsymbol{x}$.

D. Condition for Convergence

Recall that the reduced-order MM estimator employs a total of $U = \sum_{l=1}^{L} r_l + \sum_{j=1}^{J} s_j$ filters, and that the uth mode-matched filter, where $u \in \{1, 2, \ldots, U\}$ can be mapped to an element m of the process or measurement

noise. As such, let $\hat{\mu}_{\zeta_m}^{\beta,m}(k)$ denote the estimated mode probability in the reduced-order MM estimator, which maps to $\hat{\mu}_{i_m}^{q,m}(k)$ if $u \leq \sum_{l=1}^{L} r_l$, or to $\hat{\mu}_{l_m}^{r,m}(k)$ otherwise. Moreover, let $\hat{M}_{\zeta_m}^{\beta,m}(k)$ denote the process and measurement noise model assumed by the uth mode-matched filter, which can be obtained from (28)–(32). Using Bayes' formula, one can write $\hat{\mu}_{\zeta_m}^{\beta,m}(k)$ as

$$\begin{aligned}\hat{\mu}_{\zeta_m}^{\beta,m}(k) &= \Pr\left[\hat{M}_{\zeta_m}^{\beta,m}(k)\middle| z(k), Z^{k-1}\right] \\ &= \frac{\Pr\left[\hat{M}_{\zeta_m}^{\beta,m}(k), z(k)\middle| Z^{k-1}\right]}{\Pr\left[z(k)|\, Z^{k-1}\right]} \\ &= \frac{\Pr\left[z(k)|\,\hat{M}_{\zeta_m}^{\beta,m}(k), Z^{k-1}\right]\Pr\left[\hat{M}_{\zeta_m}^{\beta,m}(k)\middle| Z^{k-1}\right]}{\sum_{\zeta_n}\Pr\left[z(k)|\hat{M}_{\zeta_n}^{\beta,m}(k), Z^{k-1}\right]\Pr\left[\hat{M}_{\zeta_n}^{\beta,m}(k)\middle| Z^{k-1}\right]}.\end{aligned} \tag{42}$$

Note that $\Pr\left[\hat{M}_{\zeta_m}^{\beta,m}(k)|Z^{k-1}\right]$ is not known but if the model estimate does not vary significantly between time steps, it can be approximated with

$$\begin{aligned}\Pr\left[\hat{M}_{\zeta_m}^{\beta,m}(k)\middle| Z^{k-1}\right] &\approx \Pr\left[\hat{M}_{\zeta_m}^{\beta,m}(k-1)\middle| Z^{k-1}\right] \\ &= \hat{\mu}_{\zeta_m}^{\beta,m}(k-1)\end{aligned} \tag{43}$$

hence the following recursion is obtained:

$$\hat{\mu}_{\zeta_m}^{\beta,m}(k) \approx \alpha_{\zeta_m}^{\beta,m}(k) \cdot \hat{\mu}_{\zeta_m}^{\beta,m}(k-1) \tag{44}$$

where

$$\alpha_{\zeta_m}^{\beta,m}(k) \triangleq \frac{\Pr\left[z(k)|\,\hat{M}_{\zeta_m}^{\beta,m}(k), Z^{k-1}\right]}{\sum_{\zeta_n}\Pr\left[z(k)|\hat{M}_{\zeta_n}^{\beta,m}(k), Z^{k-1}\right]\hat{\mu}_{\zeta_n}^{\beta,m}(k-1)}. \tag{45}$$

It is required for these probabilities to converge to the right ones, i.e., all converge to zero except $\{\hat{\mu}_{n_l}^{q,l}(k)\}_{l=1}^{L}$ and $\{\hat{\mu}_{s_j}^{r,j}(k)\}_{j=1}^{L}$ converge to one. A sufficient condition for this convergence to happen is that there exists some k_0 such that $\forall\, k \geq k_0$, the following holds:

$$\underset{\zeta_m}{\text{argmax}}\left[\alpha_{\zeta_m}^{\beta,m}(k)\right] = \begin{cases} n_m, & \text{if } u \leq \sum_{l=1}^{L} r_l \\ o_m, & \text{otherwise}\end{cases} \tag{46}$$

where n_m and o_m are the indexes of the true modes of the mth process noise and measurement noise elements, respectively. The abovementioned condition is similar to

$$\underset{\zeta_m}{\text{argmax}}\left\{\Pr\left[z(k)|\hat{M}_{\zeta_m}^{\beta,m}(k), Z^{k-1}\right]\right\} = \begin{cases} n_m, & \text{if } u \leq \sum_{l=1}^{L} r_l \\ o_m, & \text{otherwise.}\end{cases} \tag{47}$$

$\forall\, k \geq k_0$, since $\sum_{\zeta_n}\Pr\left[z(k)|\hat{M}_{\zeta_n}^{\beta,m}(k), Z^{k-1}\right]\hat{\mu}_{\zeta_n}^{\beta,m}(k-1)$ is a constant with respect to ζ_m. The condition in (46) says that at each time step $k \geq k_0$, the closest constructed model to the true model is the one matched to n_m, if $u \leq \sum_{l=1}^{L} r_l$ or o_m otherwise. Note that the reduced order MM estimator can be viewed as a standard MM estimator whose mode models are different than the true model. In such cases, when the assumed modes in the standard MM estimator do not contain the true mode of the system, it has been proven in [67] that the standard MM estimator will converge to the mode whose model is the closest to the true model. As such, if (46) holds, then (38) and (39) will be satisfied and the reduced-order MM estimator will converge to the matched KF. It is important to also note that the sufficient condition in (47) holds only when the process and measurement noise statistics are statics, i.e., no mode switching is happening. A summary of the reduced-order MM algorithm is given in Fig. 2.

REMARK Intuitively, the condition in (46) is more likely to be satisfied when the models of different modes are "different" enough. For example, assuming only 1 scalar process noise element with two possible models, then (46) is more likely to hold when $|Q_1 - Q_2| = 10$ rather than $|Q_1 - Q_2| = 0.01$.

IV. SIMULATION RESULTS

It is important to note that the proposed reduced-order MM estimator is a different algorithm than the standard MM altogether. As such, one should not expect the same performance as the standard MM estimator. A sufficient condition for the reduced-order MM to achieve optimality was presented in Section III-D; however, this condition may not always be satisfied. In such cases, characterizing the loss in performance quickly becomes intractable and is left for future work. This article resorts to simulations to characterize the performance of the reduced-MM estimator. To this end, the following system is considered:

$$\boldsymbol{x}(k+1) = \begin{bmatrix}1 & T \\ 0 & 1\end{bmatrix}\boldsymbol{x}(k) + \boldsymbol{w}(k) \tag{48}$$

$$z(k) = [0.02 \quad 0.1]\,\boldsymbol{x}(k) + v(k) \tag{49}$$

where $T = 0.1$ s is the sampling time; $\boldsymbol{x} = [x_1, x_2]^{\mathrm{T}}$ is the state vector, where x_1 is expressed in meters and x_2 in meters per second; $\boldsymbol{w}$ is a zero-mean white sequence with covariance $\mathbf{Q}$ given by

$$\mathbf{Q} = \sum_{l=1}^{2} \mathbf{\Gamma}_l \mathbf{Q}^l \mathbf{\Gamma}_l^{\mathrm{T}} \tag{50}$$

where

$$\mathbf{\Gamma}_1 \triangleq [1 \quad 0]^{\mathrm{T}}, \qquad \mathbf{Q}^1 \triangleq S_1 T$$

$$\mathbf{\Gamma}_2 \triangleq \mathbf{I}_{2\times 2}, \qquad \mathbf{Q}^2 \triangleq \begin{bmatrix} S_2\frac{T^3}{3} & S_2\frac{T^2}{2} \\ S_2\frac{T^2}{2} & S_2 T\end{bmatrix}$$

the power spectra S_1 and S_2 are from the sets $\mathcal{S}_1 = \{0.1, 4, 8\}$ and $\mathcal{S}_2 = \{0.001, 0.4, 5\}$, respectively; and $v(k)$ is a zero-mean white Gaussian random variable with variance R from the set $\mathcal{R} = \{1, 8, 10\}$. It can be clearly seen that the system defined in (48) and (49) is in the form of the one defined in (1) and (2) with two process noise elements and one measurement noise element, each of which can be in one of three modes. As such, $3^2 \times 3^1 = 27$ filters are needed to implement a standard MM estimator, while only

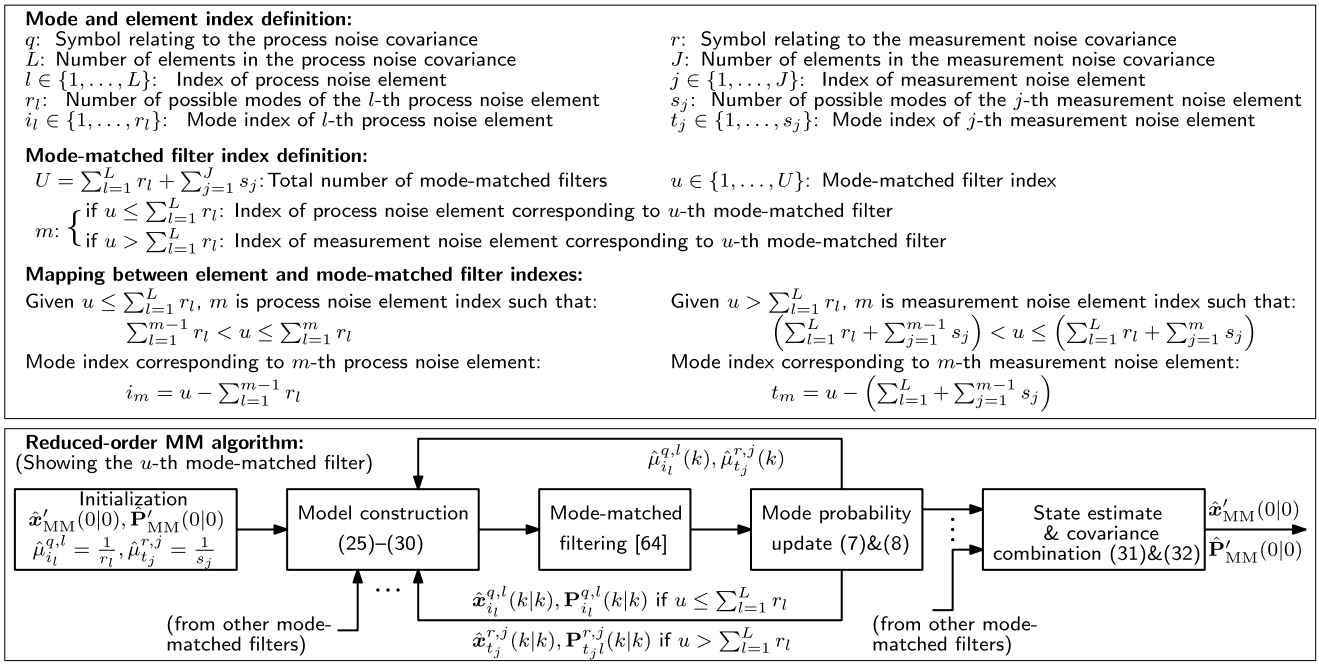

Fig. 2. Summary of the reduced-order algorithm showing how the indexes are defined and calculated as well as a block diagram of the filtering steps.

$(2 \times 3) + (1 \times 3) = 9$ filters are needed for the reduced-order MM estimator. The true system model is set to be $S_1 = 4$, $S_2 = 0.4$, and $R = 8$. The initial state statistics are chosen as $\boldsymbol{x} \sim \mathcal{N}(\boldsymbol{x}_0, \mathbf{P}_0)$, where $\boldsymbol{x}_0 \triangleq [2,\ 1]^{\mathrm{T}}$ and $\mathbf{P}_0 \triangleq \mathrm{diag}[1000,\ 10]$. Then, five estimators are implemented for comparative analysis.

1) *Matched KF:* A single KF matched to the true model.
2) *Standard MM estimator:* A standard MM estimator running all 27 filters each matched to a combination from the set $\mathcal{S}_1 \times \mathcal{S}_2 \times \mathcal{R}$.
3) *Reduced-order MM estimator:* The proposed reduced-order MM estimator with nine filters, which is the efficient implementation of the standard MM estimator.
4) *Mismatched KF—min Q:* A single KF assuming $S_1 = 0.1$, $S_2 = 0.001$, and $R = 1$.
5) *Mismatched KF—max Q:* A single KF assuming $S_1 = 8$, $S_2 = 5$, and $R = 10$.

The RMSE of each of the states x_1 and x_2 was computed from 10^4 Monte Carlo realizations for each filter and are shown in Fig. 3 along with the RMSE calculated by propagating the Riccati equation. It can be clearly seen from Fig. 3 that while the matched KF yields the lowest RMSE matching the theoretical RMSE obtained by the Riccati equation, the standard, and reduced-order MM estimators achieve comparable performance. The mismatched KF with maximum $\mathbf{Q}$ yields acceptable RMSE for x_1; however, the RMSE for x_2 is significantly large. The fraction of increase in the final RMSEs of the reduced-order MM from the standard MM estimator are 1.40% and 1.90% for x_1 and x_2, respectively. This small loss in performance between the reduced-order and standard MM estimator comes at

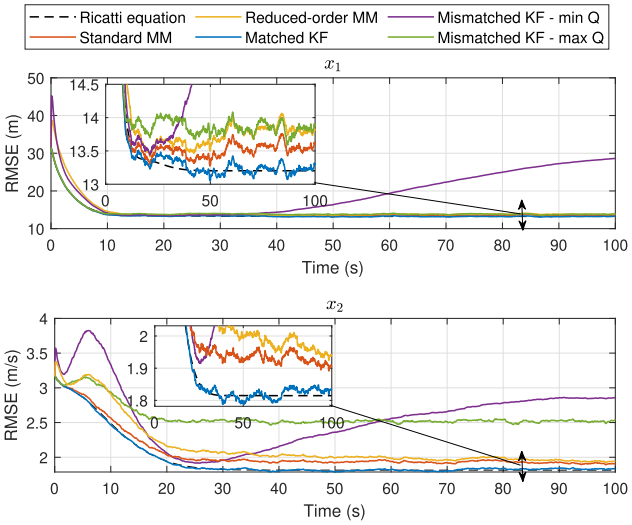

Fig. 3. Monte Carlo simulations results showing the RMSE for each error state x_1 and x_2 computed from 10^4 realizations for each of the estimators for $\mathcal{S}_1 = \{0.1, 4, 8\}$, $\mathcal{S}_2 = \{0.001, 0.4, 5\}$, and $\mathcal{R} = \{1, 8, 10\}$. The RMSE was also calculated by propagating the Riccati equation and plotted for comparison.

the benefit of a significant reduction in the number of filters needed, which in this case is a 300% reduction. The fraction of realizations in which the standard MM estimator converged to the wrong modes was 12.8% and 24.01% for the reduced-order MM estimator. Moreover, the fraction of realizations the reduced-order MM estimator converged to different modes than the standard estimator was computed to be 14.82%.

In order to explore the case where the reduced-order MM fails to approximate the standard MM, the sets $\mathcal{S}_1$, $\mathcal{S}_2$,

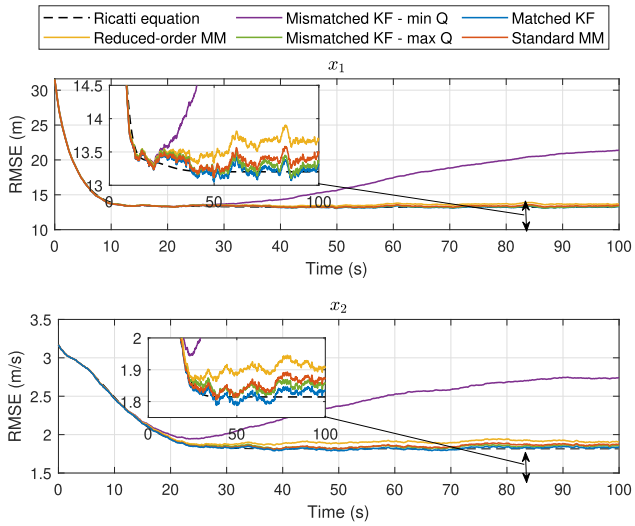

Fig. 4. Monte Carlo simulations results showing the RMSE for each error state x_1 and x_2 computed from 10^4 realizations for each of the estimators for $\mathcal{S}_1 = \{3.5, 4, 8\}$, $\mathcal{S}_2 = \{0.01, 0.4, 0.8\}$, and $\mathcal{R} = \{6, 8, 10\}$. The RMSE was also calculated by propagating the Riccati equation and plotted for comparison.

and $\mathcal{R}$ are changed to $\mathcal{S}_1 = \{3.5, 4, 8\}$, $\mathcal{S}_2 = \{0.01, 0.4, 8\}$, and $\mathcal{R} = \{6, 8, 10\}$. Then, the following five estimators are implemented for comparative analysis.

1) *Matched KF:* A single KF matched to the true model.
2) *Standard MM estimator:* A standard MM estimator running all 27 filters each matched to a combination from the set $\mathcal{S}_1 \times \mathcal{S}_2 \times \mathcal{R}$.
3) *Reduced-order MM estimator:* The proposed reduced-order MM estimator with 9 filters, which is the efficient implementation of the standard MM estimator.
4) *Mismatched KF—min Q:* A single KF assuming $S_1 = 3.4$, $S_2 = 0.01$, and $R = 6$.
5) *Mismatched KF—max Q:* A single KF assuming $S_1 = 8$, $S_2 = 0.8$, and $R = 10$.

The new results are shown in Fig. 4 . As can be seen from the figure, when there is less distinction between the modes, reflected by the fact that the values in $\mathcal{S}_1$, $\mathcal{S}_2$, and $\mathcal{R}$ are now closer to one another, the reduced-order MM struggles to properly approximate the standard MM. This is an indication that the sufficient condition discussed in Section III-D is not satisfied. Although the reduced-order MM performed worse after changing $\mathcal{S}_1$ and $\mathcal{S}_2$, it still yielded acceptable performance, especially compared to the mismatched KF with the minimum $\mathbf{Q}$. The mismatched KF with the maximum $\mathbf{Q}$ yields acceptable RMSEs. This second set of simulation results highlights the importance of the condition in Section III-D for both MM estimators and suggest that when the modes are "close enough," there is not much gain in using an MM estimation approach over the maximum $\mathbf{Q}$ filter. However, in practical MM applications, the modes will be significantly distinct. In such cases, the reduced-order MM would be desirable as it performs similarly to the standard MM estimator but with the fraction of its complexity. This is illustrated in the following section. The simulation results are summarized in Table I .

TABLE I
Summary of Simulation 1/Simulation 2 Results

Estimator	Number of filters	Final RMSE for x_1 (m)	Final RMSE for x_2 (m/s)
Matched KF	1	13.32/13.32	1.835/1.835
Mismatched KF−max Q	1	13.91/13.38	2.532/1.858
Mismatched KF−min Q	1	28.63/21.39	2.861/2.744
Standard MM	27	13.79/13.51	1.893/1.874
Reduced-order MM	9	13.83/13.71	1.943/1.910

V. CASE STUDY: UAV NAVIGATION WITH CELLULAR SOPS

This section presents experimental results for the case of UAV navigation with SOPs to validate the proposed method.

A. System Model

In what follows, the UAV motion model, clock error models, and measurement models are described and the mode-matched EKFs are formulated.

1) *UAV Dynamics Model:* The UAV's 2-D position and velocity states, $\boldsymbol{r}_r$ and $\dot{\boldsymbol{r}}_r$, respectively, are assumed to evolve according to velocity random walk dynamics. Note that it is assumed that the UAV knows its altitude from other sensors, such as a barometric altimeter. As such, the discrete-time dynamics of $\boldsymbol{x}_{\text{pv}} \triangleq [\boldsymbol{r}_r^{\text{T}}, \dot{\boldsymbol{r}}_r^{\text{T}}]^{\text{T}}$ will be given by

$$\boldsymbol{x}_{\text{pv}}(k+1) = \mathbf{F}_{\text{pv}}\boldsymbol{x}_{\text{pv}}(k) + \boldsymbol{w}_{\text{pv}}(k), \quad , k = 0, 1, \ldots \tag{51}$$

where $\boldsymbol{w}_{\text{pv}}$ is a zero-mean, white sequence with covariance $\mathbf{Q}_{\text{pv}}$, and

$$\mathbf{F}_{\text{pv}} \triangleq \begin{bmatrix} \mathbf{I}_{2\times 2} & T\mathbf{I}_{2\times 2} \\ \mathbf{0}_{2\times 2} & \mathbf{I}_{2\times 2} \end{bmatrix}, \quad \mathbf{Q}_{\text{pv}} \triangleq \begin{bmatrix} \frac{T^3}{3}\tilde{\mathbf{S}}_{\text{pv}} & \frac{T^2}{2}\tilde{\mathbf{S}}_{\text{pv}} \\ \frac{T^2}{2}\tilde{\mathbf{S}}_{\text{pv}} & T\tilde{\mathbf{S}}_{\text{pv}} \end{bmatrix}$$

where T is the sampling interval, $\tilde{\mathbf{S}}_{\text{pv}} \triangleq \text{diag}[\tilde{q}_x, \tilde{q}_y]$, and $\tilde{q}_x$ and $\tilde{q}_y$ are the x and y acceleration noise power spectra, respectively.

2) *Clock Error Dynamics Model:* Let $\boldsymbol{x}_{\text{clk}_n} \triangleq c[\delta t_n, \dot{\delta} t_n]^{\text{T}}$ denote the clock error state of the nth BTS, where δt_n is the difference between the BTS's and receiver's clock biases, $\dot{\delta} t_n$ is the difference of their drifts, and c is the speed of light. A double integrator driven by process noise is used to model each of the clock error states. As such, $\boldsymbol{x}_{\text{clk}_n}$ will evolve according to

$$\boldsymbol{x}_{\text{clk}_n}(k+1) = \mathbf{F}_{\text{clk}}\boldsymbol{x}_{\text{clk}_n}(k) + \boldsymbol{w}_{\text{clk}_n}(k) \tag{52}$$

where $\boldsymbol{w}_{\text{clk}_n}$ is a zero-mean, white sequence with covariance $\mathbf{Q}_{\text{clk}_n} \triangleq \mathbf{Q}_{\text{clk}_r} + \mathbf{Q}_{\text{clk}_{s_n}}$, and

$$\mathbf{F}_{\text{clk}} \triangleq \begin{bmatrix} 1 & T \\ 0 & 1 \end{bmatrix}, \quad \mathbf{Q}_{\text{clk}_i} \triangleq \begin{bmatrix} \frac{T^3}{3}\tilde{S}_{\dot{\delta} t_i} + T\tilde{S}_{\delta t_i} & \frac{T^2}{2}\tilde{S}_{\dot{\delta} t} \\ \frac{T^2}{2}\tilde{S}_{\dot{\delta} t_i} & T\tilde{S}_{\dot{\delta} t_i} \end{bmatrix}$$

where $\tilde{S}_{\delta t_i}$ and $\tilde{S}_{\dot{\delta} t_i}$ are the clock bias and clock drift process noise power spectra, and i denotes either the receiver-mounted UAV r or the nth BTS s_n. The power spectra

$\tilde{S}_{\delta t_i}$ and $\tilde{S}_{\dot{\delta} t_i}$ can be related to the power-law coefficients $\{h_\alpha\}_{\alpha=-2}^{2}$, which have been shown through laboratory experiments to characterize the power spectral density of the fractional frequency deviation $y(t)$ of an oscillator from nominal frequency, namely, $\tilde{S}_y(f) = \sum_{\alpha=-2}^{2} h_\alpha f^\alpha$ [68]. It is common to approximate such relationships by considering only the frequency random-walk coefficient h_{-2} and the white frequency coefficient h_0, which lead to $\tilde{S}_{\delta t_i} \approx h_{0,i}$ and $\tilde{S}_{\dot{\delta} t_i} \approx 2\pi^2 h_{-2,i}$ [66], [69]. It is important to note that the process noise in the clock error states will be correlated due to receiver's process noise; hence

$$\mathbb{E}\left[\boldsymbol{w}_{\mathrm{clk}_n}(k)\boldsymbol{w}_{\mathrm{clk}_n}^{\mathsf{T}}(k)\right] = \begin{cases} \mathbf{Q}_{\mathrm{clk}_r} + \mathbf{Q}_{\mathrm{clk}_{s_n}}, & \text{if } n = m \\ \mathbf{Q}_{\mathrm{clk}_r}, & \text{otherwise.} \end{cases} \tag{53}$$

3) *Measurement Model:* Carrier phase measurements are more precise than pseudorange measurements [70] and will be, hence, used in what follows. Note that the precision of carrier phase measurements come at the price of additional ambiguities, which have been shown lumped into the clock biases δt_n. The carrier phase measurement expressed in meters can be modeled as

$$z_n(k) = \left\|\boldsymbol{r}_r(k) - \boldsymbol{r}_{s_n}\right\|_2 + c\delta t_n(k) + v_n(k) \tag{54}$$

where $\boldsymbol{r}_{s_n}$ is the nth BTS's known 2-D position vector and $v_n(k)$ is the measurement noise, which is modeled as a zero mean, white Gaussian random variable with variance $\sigma_n^2(k)$. The statistics of $v_n(k)$ are discussed in [70].

4) *EKF Model:* The EKF estimates the UAV-mounted receiver's position and velocity and the clock error states for all BTSs, namely

$$\boldsymbol{x}(k) \triangleq \left[\boldsymbol{x}_{\mathrm{pv}}^{\mathsf{T}}(k), \boldsymbol{x}_{\mathrm{clk}_1}^{\mathsf{T}}(k), \ldots, \boldsymbol{x}_{\mathrm{clk}_N}^{\mathsf{T}}(k)\right]^{\mathsf{T}} \tag{55}$$

where N is the total number of available BTSs. As such, it follows that the dynamics of $\boldsymbol{x}$ and the measurement model will be given by

$$\boldsymbol{x}(k+1) = \mathbf{F}\boldsymbol{x}(k) + \boldsymbol{w}(k) \tag{56}$$

$$\boldsymbol{z}(k) = \boldsymbol{h}\left[\boldsymbol{x}(k)\right] + \boldsymbol{v}(k) \tag{57}$$

where $\mathbf{F} \triangleq \mathrm{diag}[\mathbf{F}_{\mathrm{pv}}, \mathbf{F}_{\mathrm{clk}}, \ldots, \mathbf{F}_{\mathrm{clk}}]$; $\boldsymbol{h}[\boldsymbol{x}(k)] \triangleq [h_1[\boldsymbol{x}(k)], \ldots, h_N[\boldsymbol{x}(k)]]^{\mathsf{T}}$, $h_n[\boldsymbol{x}(k)] \triangleq \|\boldsymbol{r}_r(k) - \boldsymbol{r}_{s_n}\|_2 + c\delta t_n(k)$, $\boldsymbol{z}(k) \triangleq [z_1(k), \ldots, z_N(k)]^{\mathsf{T}}$; $\boldsymbol{w}(k)$ is a discrete-time zero-mean white sequence with covariance $\mathbf{Q} \triangleq \mathrm{diag}[\mathbf{Q}_{\mathrm{pv}}, \mathbf{Q}_{\mathrm{clk}}]$

$$\mathbf{Q}_{\mathrm{clk}} \triangleq \begin{bmatrix} \mathbf{Q}_{\mathrm{clk},r}+\mathbf{Q}_{\mathrm{clk},1} & \mathbf{Q}_{\mathrm{clk},r} & \cdots & \mathbf{Q}_{\mathrm{clk},r} \\ \mathbf{Q}_{\mathrm{clk},r} & \mathbf{Q}_{\mathrm{clk},r}+\mathbf{Q}_{\mathrm{clk},2} & \cdots & \mathbf{Q}_{\mathrm{clk},r} \\ \vdots & \vdots & \ddots & \vdots \\ \mathbf{Q}_{\mathrm{clk},r} & \mathbf{Q}_{\mathrm{clk},r} & \cdots & \mathbf{Q}_{\mathrm{clk},r}+\mathbf{Q}_{\mathrm{clk},N} \end{bmatrix}$$

and $\boldsymbol{v}(k) \triangleq [v_1(k), \ldots, v_N(k)]^{\mathsf{T}}$ is a discrete-time zero-mean white Gaussian sequence with covariance $\mathbf{R}(k) \triangleq \mathrm{diag}[\sigma_1^2(k), \ldots, \sigma_N^2(k)]$. It can be readily seen that $\mathbf{Q}$ is of the form defined in (3), particularly, it can be expressed as

$$\mathbf{Q} = \mathbf{\Gamma}_{\mathrm{pv}}\mathbf{Q}_{\mathrm{pv}}\mathbf{\Gamma}_{\mathrm{pv}}^{\mathsf{T}} + \mathbf{\Gamma}_r\mathbf{Q}_{\mathrm{clk}_r}\mathbf{\Gamma}_r^{\mathsf{T}} + \sum_{n=1}^{N} \mathbf{\Gamma}_{s_n}\mathbf{Q}_{\mathrm{clk}_{s_n}}\mathbf{\Gamma}_{s_n}^{\mathsf{T}} \tag{58}$$

where $\mathbf{\Gamma}_{\mathrm{pv}} \triangleq [\mathbf{I}_{4\times4}, \mathbf{0}_{4\times2N}]^{\mathsf{T}}$, $\mathbf{\Gamma}_r \triangleq [\mathbf{0}_{2\times4}, \mathbf{I}_{2\times2}, \ldots, \mathbf{I}_{2\times2}]^{\mathsf{T}}$, and $\mathbf{\Gamma}_{s_n} \triangleq [\mathbf{0}_{2\times4}, \mathbf{0}_{2\times2}, \ldots, \mathbf{0}_{2\times2}, \mathbf{I}_{2\times2}, \mathbf{0}_{2\times2}, \ldots, \mathbf{0}_{2\times2}]^{\mathsf{T}}$. Each EKF is producing an estimate $\hat{\boldsymbol{x}}(k|j) = \mathbb{E}[\boldsymbol{x}(k)|\boldsymbol{z}(1), \ldots, \boldsymbol{z}(j)]$, $j \leq k$, with an associated estimation error covariance $\mathbf{P}(k|j) = \mathbb{E}[\tilde{\boldsymbol{x}}(k|j)\tilde{\boldsymbol{x}}^{\mathsf{T}}(k|j)]$, where $\tilde{\boldsymbol{x}}(k|j) \triangleq \boldsymbol{x}(k) - \hat{\boldsymbol{x}}(k|j)$ is the estimation error. The current state estimate $\hat{\boldsymbol{x}}(k|k)$ and its associated estimation error covariance $\mathbf{P}(k|k)$ are obtained using the standard EKF equations. It has been proven in [70] that the system in (56) and (57) is observable for $N \geq 2$ and the estimation error will be bounded in a mean-squared sense. The measurement Jacobian $\mathbf{H}(k)$ used in the EKF estimation error covariance update is given by

$$\mathbf{H}(k) = \begin{bmatrix} \mathbf{G}(k) & \mathbf{I}_{N\times N} & \mathbf{0}_{(N+2)\times(N+2)} \end{bmatrix} \tag{59}$$

$$\mathbf{G}(k) \triangleq \begin{bmatrix} \frac{\boldsymbol{r}_r(k)-\boldsymbol{r}_{s_1}}{\|\boldsymbol{r}_r(k)-\boldsymbol{r}_{s_1}\|_2} & \cdots & \frac{\boldsymbol{r}_r(k)-\boldsymbol{r}_{s_N}}{\|\boldsymbol{r}_r(k)-\boldsymbol{r}_{s_N}\|_2} \end{bmatrix}^{\mathsf{T}} \tag{60}$$

where $\mathbf{G}(k)$ is evaluated at $\hat{\boldsymbol{x}}(k|j)$. As such, linearizing the system defined in (56) and (57) around the estimate yields

$$\tilde{\boldsymbol{x}}(k+1|k) = \mathbf{F}\tilde{\boldsymbol{x}}(k|k) + \boldsymbol{w}(k) \tag{61}$$

$$\boldsymbol{v}(k) = \mathbf{H}(k)\tilde{\boldsymbol{x}}(k|k-1) + \boldsymbol{v}(k) \tag{62}$$

where $\boldsymbol{v}(k) \triangleq \boldsymbol{z}(k) - \boldsymbol{h}[\hat{\boldsymbol{x}}(k|k-1)]$ is the innovation vector. The system in (61) and (62) is an LTV system whose process noise covariance given in (58) is of the form in (3). Consequently, the proposed reduced-order MM estimator can be used to estimate $\boldsymbol{x}$.

B. Hardware Setup and Filter Description

For this experiment, a DJI Matrice 600 was equipped with an Ettus E312 universal software radio peripheral (USRP), a consumer-grade 800/1900 MHz cellular antenna, and a small consumer-grade GPS antenna to discipline the on-board oscillator. The UAV-mounted receiver was tuned to listen to cellular signals in the 800 MHz band allocated for cellular communication in the U.S. Specifically, the E312 USRP was tuned to an 882.75 MHz carrier frequency, which is a cellular CDMA channel allocated for the U.S. cellular provider Verizon Wireless. Samples of the received signals were stored for offline postprocessing. The cellular carrier phase measurements were given at a rate of 37.5 Hz, i.e., $T = 26.67$ ms. The ground-truth reference for the UAV trajectory was taken from its on-board navigation system, which uses GPS, an inertial measurement unit, and other sensors. The hovering horizontal precision of the UAV is reported to be 1.5 m by DJI. The x and y continuous-time acceleration noise spectra were set to $\tilde{q}_x = \tilde{q}_y = 0.03\,\mathrm{m}^2/\mathrm{s}^3$. Throughout the experiment, the receiver on-board the UAV was listening to 7 cellular CDMA BTSs whose positions were determined beforehand. The experimental setup and BTS layout is shown in Fig. 5.

In this experiment, the statistics of the process noise driving the receiver and BTS clocks are unknown. The qualities of the BTS clock oscillators are assumed to range between that of a typical oven-controlled crystal oscillator (OCXO) and that of a high-quality OCXO. The quality of the receiver clock oscillator is assumed to range between

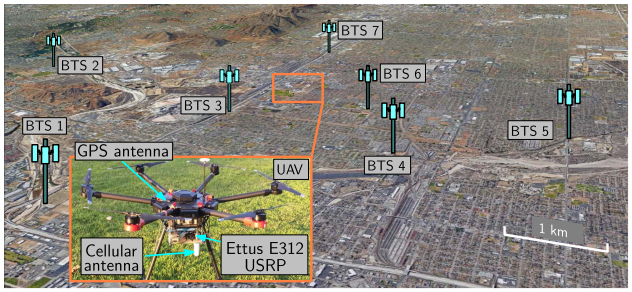

Fig. 5. Experimental setup and BTS layout. The environment consists of 7 cellular CDMA BTSs.

TABLE II
Oscillator Parameters

Parameter	Value
High-quality OCXO $\{h_0, h_{-2}\}$	$\{2.6 \times 10^{-22}, 4.0 \times 10^{-26}\}$
Typical OCXO $\{h_0, h_{-2}\}$	$\{8.0 \times 10^{-20}, 4.0 \times 10^{-23}\}$
Typical TCXO $\{h_0, h_{-2}\}$	$\{9.4 \times 10^{-20}, 3.8 \times 10^{-21}\}$

TABLE III
Position RMSEs and Final Errors

Estimator	Number of filters	RMSE	Final error
Standard EKF	1	38.76 m	40.03 m
Standard MM	256	5.73 m	6.21 m
Reduced-order MM	16	5.67 m	6.25 m

that of a typical temperature compensated crystal oscillator (TCXO) and that of a typical OCXO. As such, each clock error state is assumed to be in one of two modes. The h_0 and h_{-2} parameters of the aforementioned oscillators are given in Table II. Three estimators of $\boldsymbol{x}$ are implemented for a comparative study.

1) *Standard EKF:* A single EKF matched to a typical TCXO for the receiver clock and typical OCXOs for the BTSs' clocks.
2) *Standard MM estimator:* A standard MM estimator running $2^8 = 256$ filters each matched to a combination of typical TCXO or OCXO for the receiver clock and typical or high-quality OCXO for the BTSs' clocks.
3) *Reduced-order MM estimator:* The proposed reduced-order MM estimator with $2 \times 8 = 16$ filters, which is the efficient implementation of the standard MM estimator.

Each EKF was initialized according to the framework in [70] with initial position estimates obtained from the UAVs' on-board navigation systems and with equal mode probabilities.

C. Experimental Results and Discussion

The UAV's total traversed trajectory was 3.02 km, which was completed in 320 s. The true and estimated UAV trajectories are shown in Fig. 6. The total position RMSE

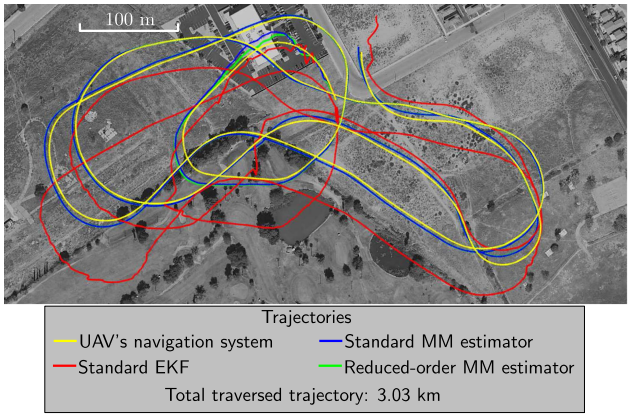

Fig. 6. True UAV trajectory and estimated UAV trajectories via the three estimators. Map data: Google Earth.

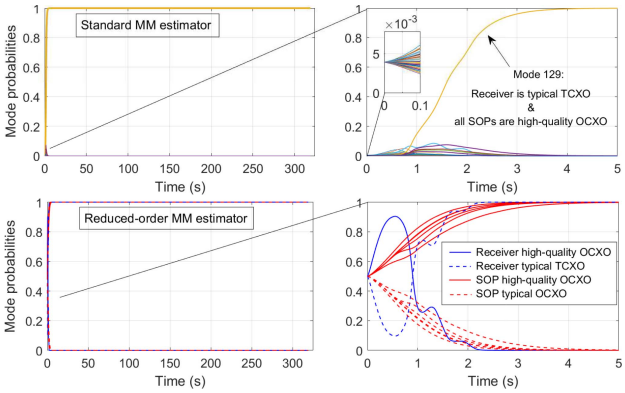

Fig. 7. Time history of the probabilities of the standard and reduced-order MM estimators.

was calculated for each estimator is tabulated in Table III along with the final estimation errors.

It can be seen from Fig. 6 and Table III that both MM estimators perform significantly better than the standard EKF. The time history of the mode probabilities for the standard MM and reduced-order MM estimators shown in Fig. 7 shed light on why both MM estimators performed significantly better than the standard EKF. It can be seen from Fig. 7 that all mode probabilities in the standard MM estimator converged to zero, except for that of mode 129, which corresponds to the receiver clock being a typical TCXO and all BTSs' clocks being high-quality OCXOs. Convergence happened within the first 5 s of the experiment. That is, throughout the remaining 315 s, the standard MM behaved as a single EKF matched to mode 129. In contrast, the standard EKF considered in this experiment was matched to a receiver clock being a typical TCXO while the BTS clocks were assumed to be typical OCXOs. The model assumed by the standard EKF apparently mismatches the true model, resulting in large EKF errors. Such large errors were mitigated by the standard MM which converged to mode 129, indicating that the true model is closer to the one of mode 129 than the one assumed by the standard EKF. What is more interesting is that the reduced-order MM estimator mode probabilities converged to the same

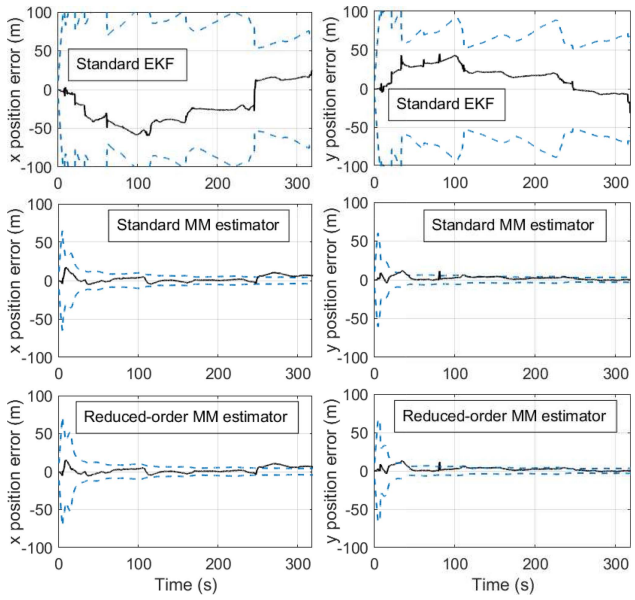

Fig. 8. UAV's position estimation error trajectories (solid black lines) and associated $\pm 3\sigma$ bounds (dashed blue lines) for each estimator.

values as the standard MM. That is, the probability of the receiver clock being a typical TCXO converged to 1 and the probability of all BTSs' clocks being OCXOs converged to 1 as well. In other words, the reduced-order MM also behaved as a single EKF matched to mode 129 after convergence. Consequently, one should expect that after some transient, the reduced-order MM estimator should converge to the standard MM estimator. This can be seen in Fig. 6, where the green curve (from the reduced-order MM estimator) converges to blue one (from the standard MM estimator) after some transient. This is also reflected in the RMSE and final error values in Table III. To see this even more, the EKF position errors and the associated $\pm 3\sigma$ bounds are shown in Fig. 8 for each estimator. A closer look at the EKF errors and $\pm 3\sigma$ bounds of both MM estimators shows small differences in the first few seconds and almost identical behavior afterwards.

VI. CONCLUSION

A reduced-order MM estimator for static noise identification in dynamic stochastic systems was proposed. The proposed algorithm reduces the computational complexity of MM estimation from exponential to polynomial by constructing a significantly smaller set of mode models which are updated every time step. It is assumed that the constructed mode models do not change significantly between time steps, which can be guaranteed by the smoothness of the mode probabilities. It is shown that the reduced-order MM estimator converges to the standard MM estimator when the mode models are sufficiently distinct. Two sets of Monte Carlo simulations were conducted, as follows: 1) one where the mode models were significantly distinct and 2) one where mode models were very close. In the first set of simulations, the reduced-order MM estimator performs nearly similar to the standard MM estimator while some degradation is observed in the second set. However, the reduced-order MM yielded acceptable performance in both simulation sets and was implemented with a fraction of the standard MM estimator's complexity. Experimental results of opportunistic navigation on a UAV in the case of unknown transmitter clock process noise covariances were also presented to further validate the proposed approach. The experimental results show a UAV navigating for more than 5 min over a trajectory of more than 3 km, with a final position error of 6.21 m obtained using the standard MM estimator versus a final position error of 6.25 m obtained using the proposed reduced-order MM estimator. A standard EKF was implemented for comparative analysis, showing a final error of 40.03 m. In the experiments, the reduced-order MM estimator was implemented with 16 filters, while the standard MM was implemented with 256 filters. While the proposed approach is showing promising results when the mode models are significantly distinct, a necessary condition for optimality is needed and is left as future work.

APPENDIX
PROOF OF LEMMA III.1

This appendix provides the proof of Lemma III.1.

PROOF Note the marginalization

$$\begin{aligned}
&\sum_{t_1}\cdots\sum_{t_J}\mu_{i_1,\ldots,i_L,t_1,\ldots,t_J}(k)\\
&\quad=\sum_{t_1}\cdots\sum_{t_J}\Pr\left[M_{i_1}^1,\ldots,M_{i_L}^L,N_{t_1}^1,\ldots,N_{t_J}^J\middle|Z^k\right]\\
&\quad=\Pr\left[M_{i_1}^1,\ldots,M_{i_L}^L\middle|Z^k\right]\\
&\quad\triangleq\mu_{i_1,\ldots,i_L}^q(k). \qquad (63)
\end{aligned}$$

Using (63), (20) becomes

$$\begin{aligned}
\hat{\mathbf{Q}}(k)=&\sum_{i_1}\cdots\sum_{i_L}\mu_{i_1,\ldots,i_L}^q(k)\boldsymbol{\Gamma}_1\mathbf{Q}_{i_1}^1\boldsymbol{\Gamma}_1^{\mathrm{T}}+\cdots\\
&+\sum_{i_1}\cdots\sum_{i_L}\mu_{i_1,\ldots,i_L}^q(k)\boldsymbol{\Gamma}_L\mathbf{Q}_{i_L}^L\boldsymbol{\Gamma}_L^{\mathrm{T}}\\
=&\sum_{i_1}\boldsymbol{\Gamma}_1\mathbf{Q}_{i_1}^1\boldsymbol{\Gamma}_1^{\mathrm{T}}\sum_{i_2}\cdots\sum_{i_L}\mu_{i_1,\ldots,i_L}^q(k)+\cdots\\
&+\sum_{i_L}\boldsymbol{\Gamma}_L\mathbf{Q}_{i_L}^L\boldsymbol{\Gamma}_L^{\mathrm{T}}\sum_{i_1}\cdots\sum_{i_{L-1}}\mu_{i_1,\ldots,i_L}^q(k). \qquad (64)
\end{aligned}$$

Moreover, define the following marginal probabilities:

$$\begin{aligned}
&\sum_{i_1}\cdots\sum_{i_{l-1}}\sum_{i_{l+1}}\cdots\sum_{i_L}\mu_{i_1,\ldots,i_L}^q(k)\\
&\quad=\sum_{i_1}\cdots\sum_{i_{l-1}}\sum_{i_{l+1}}\cdots\sum_{i_L}\Pr\left[M_{i_1}^1,\ldots,M_{i_L}^L\middle|Z^k\right]\\
&\quad=\Pr\left[M_{i_l}^l\middle|Z^k\right]\\
&\quad\triangleq\mu_{i_l}^{q,l}(k). \qquad (65)
\end{aligned}$$

Subsequently, the estimated process noise covariance may be expressed as

$$\begin{aligned}\hat{\mathbf{Q}}(k)=&\sum_{i_1}\boldsymbol{\Gamma}_1\mathbf{Q}_{i_1}^1\boldsymbol{\Gamma}_1^{\mathsf{T}}\mu_{i_1}^{q,1}(k)+\cdots+\sum_{i_L}\boldsymbol{\Gamma}_L\mathbf{Q}_{i_L}^L\boldsymbol{\Gamma}_L^{\mathsf{T}}\mu_{i_L}^{q,L}(k)\\ =&\sum_{l=1}^{L}\sum_{i_l}\mu_{i_l}^{q,l}(k)\boldsymbol{\Gamma}_l\mathbf{Q}_{i_l}^l\boldsymbol{\Gamma}_l^{\mathsf{T}}=\frac{1}{L}\left[\sum_{l=1}^{L}\sum_{i_l}\mu_{i_l}^{q,l}(k)\boldsymbol{\Gamma}_l\mathbf{Q}_{i_l}^l\boldsymbol{\Gamma}_l^{\mathsf{T}}\right.\\ &\left.+\cdots+\sum_{l=1}^{L}\sum_{i_l}\mu_{i_l}^{q,l}(k)\boldsymbol{\Gamma}_l\mathbf{Q}_{i_l}^l\boldsymbol{\Gamma}_l^{\mathsf{T}}\right].\end{aligned}\tag{66}$$

Therefore

$$\begin{aligned}\hat{\mathbf{Q}}(k)=&\frac{1}{L}\left\{\left[\sum_{i_1}\mu_{i_1}^{q,1}(k)\boldsymbol{\Gamma}_1\mathbf{Q}_{i_1}^1\boldsymbol{\Gamma}_1^{\mathsf{T}}+\sum_{l=2}^{L}\sum_{i_l}\mu_{i_l}^{q,l}(k)\boldsymbol{\Gamma}_l\mathbf{Q}_{i_l}^l\boldsymbol{\Gamma}_l^{\mathsf{T}}\right]\right.\\ &+\cdots\\ &\left.+\left[\sum_{i_L}\mu_{i_L}^{q,L}(k)\boldsymbol{\Gamma}_L\mathbf{Q}_{i_L}^L\boldsymbol{\Gamma}_L^{\mathsf{T}}+\sum_{l=1}^{L-1}\sum_{i_l}\mu_{i_l}^{q,l}(k)\boldsymbol{\Gamma}_l\mathbf{Q}_{i_l}^l\boldsymbol{\Gamma}_l^{\mathsf{T}}\right]\right\}.\end{aligned}\tag{67}$$

Next, defining $\bar{\mathbf{Q}}^m(k)$ according to (26) and noting that $\sum_{i_l}\mu_{i_l}^{q,l}(k)=1$, the estimated process noise covariance becomes

$$\begin{aligned}\hat{\mathbf{Q}}(k)=&\frac{1}{L}\left[\sum_{i_1}\mu_{i_1}^{q,l}(k)\boldsymbol{\Gamma}_1\mathbf{Q}_{i_1}^1\boldsymbol{\Gamma}_1^{\mathsf{T}}+\bar{\mathbf{Q}}^1(k)\right]\\ &+\cdots+\frac{1}{L}\left[\sum_{i_L}\mu_{i_L}^{q,L}(k)\boldsymbol{\Gamma}_L\mathbf{Q}_{i_L}^L\boldsymbol{\Gamma}_L^{\mathsf{T}}+\bar{\mathbf{Q}}^L(k)\right]\\ =&\frac{1}{L}\left[\sum_{i_1}\mu_{i_1}^{q,l}(k)\boldsymbol{\Gamma}_1\mathbf{Q}_{i_1}^1\boldsymbol{\Gamma}_1^{\mathsf{T}}+\bar{\mathbf{Q}}^1(k)\sum_{i_1}\mu_{i_1}^{q,l}(k)\right]+\cdots\\ &+\frac{1}{L}\left[\sum_{i_L}\mu_{i_L}^{q,L}(k)\boldsymbol{\Gamma}_L\mathbf{Q}_{i_L}^L\boldsymbol{\Gamma}_L^{\mathsf{T}}+\bar{\mathbf{Q}}^L(k)\sum_{i_L}\mu_{i_L}^{q,L}(k)\right]\\ =&\frac{1}{L}\sum_{i_1}\mu_{i_1}^{q,1}(k)\left[\boldsymbol{\Gamma}_1\mathbf{Q}_{i_1}^1\boldsymbol{\Gamma}_1^{\mathsf{T}}+\bar{\mathbf{Q}}^1(k)\right]+\cdots\\ &+\frac{1}{L}\sum_{i_L}\mu_{i_L}^{q,L}(k)\left[\boldsymbol{\Gamma}_L\mathbf{Q}_{i_L}^L\boldsymbol{\Gamma}_L^{\mathsf{T}}+\bar{\mathbf{Q}}^L(k)\right].\end{aligned}\tag{68}$$

Defining $\bar{\mathbf{Q}}_{i_m}^m(k)$ according to (24) yields (22). A similar approach is taken for $\mathbf{R}(k)$. ■

ACKNOWLEDGMENT

The authors would like to thank J. Morales and K. Shamaei for their help with data collection.

REFERENCES

[1] C. Cadena et al., "Past, present, and future of simultaneous localization and mapping: Toward the robust-perception age," *IEEE Trans. Robot.*, vol. 32, no. 6, pp. 1309–1332, Dec. 2016.

[2] J. Choi and M. Maurer, "Local volumetric hybrid-map-based simultaneous localization and mapping with moving object tracking," *IEEE Trans. Intell. Transp. Syst.*, vol. 17, no. 9, pp. 2440–2455, Sep. 2016.

[3] J. Morales, J. Khalife, and Z. Kassas, "Information fusion strategies for collaborative inertial radio SLAM," *IEEE Trans. Intell. Transp. Syst.*, vol. 23, no. 8, pp. 12935–12952, Aug. 2022.

[4] Z. Kassas et al., "Enter LEO on the GNSS stage: Navigation with Starlink satellites," *Inside GNSS Mag.*, vol. 16, no. 6, pp. 42–51, 2021.

[5] J. Dunik, O. Straka, O. Kost, and J. Havlik, "Noise covariance matrices in state-space models: A survey and comparison of estimation methods—Part I," *Int. J. Adaptive Control Signal Process.*, vol. 31, no. 11, pp. 1505–1543, May 2017.

[6] D. Alspach and H. Sorenson, "Nonlinear Bayesian estimation using Gaussian sum approximations," *IEEE Trans. Autom. Control*, vol. AC-17, no. 4, pp. 439–448, Aug. 1972.

[7] D. Wiberg, T. Powell, and D. Ljungquist, "An online parameter estimator for quick convergence and time-varying linear systems," *IEEE Trans. Autom. Control*, vol. 45, no. 10, pp. 1854–1863, Oct. 2000.

[8] L. Zhong and C. Shing-Chow, "Adaptive fading Bayesian unscented Kalman filter and smoother for state estimation of unmanned aircraft systems," *IEEE Access*, vol. 8, pp. 119470–119486, 2020.

[9] P. Gutman and M. Velger, "Tracking targets using adaptive Kalman filtering," *IEEE Trans. Aerosp. Electron. Syst.*, vol. 26, no. 5, pp. 691–699, Sep. 1990.

[10] R. Moghe, R. Zanetti, and M. Akella, "Adaptive Kalman filter for detectable linear time invariant systems," *J. Guid. Control Dyn.*, vol. 42, no. 10, pp. 2197–2205, 2019.

[11] N. Stacey and D'. S. Amico, "Adaptive and dynamically constrained process noise estimation for orbit determination," *IEEE Trans. Aerosp. Electron. Syst.*, vol. 57, no. 5, pp. 2920–2937, Oct. 2021.

[12] P. Bélanger, "Estimation of noise covariance matrices for a linear time-varying stochastic process," *Automatica*, vol. 10, no. 3, pp. 267–275, 1974.

[13] B. Odelson, M. Rajamani, and J. Rawlings, "A new autocovariance least-squares method for estimating noise covariances," *Automatica*, vol. 42, no. 2, pp. 303–308, 2006.

[14] J. Dunik, O. Straka, and M. Simandl, "On autocovariance least-squares method for noise covariance matrices estimation," *IEEE Trans. Autom. Control*, vol. 62, no. 2, pp. 967–972, Feb. 2017.

[15] R. Kashyap, "Maximum likelihood identification of stochastic linear systems," *IEEE Trans. Autom. Control*, vol. AC-15, no. 1, pp. 25–34, Feb. 1970.

[16] R. Shumway and D. Stoffer, "An approach to time series smoothing and forecasting using the EM algorithm," *J. Time Ser. Anal.*, vol. 3, no. 4, pp. 253–264, Jul. 1982.

[17] V. Bavdekar, A. Deshpande, and S. Patwardhan, "Identification of process and measurement noise covariance for state and parameter estimation using extended Kalman filter," *J. Process Control*, vol. 21, no. 4, pp. 585–601, 2011.

[18] R. Mehra, "Approaches to adaptive filtering," *IEEE Trans. Autom. Control*, vol. AC-17, no. 5, pp. 693–698, Oct. 1972.

[19] S. Sarkka and A. Nummenmaa, "Recursive noise adaptive Kalman filtering by variational Bayesian approximations," *IEEE Trans. Autom. Control*, vol. 3, no. 4, pp. 596–600, Mar. 2009.

[20] Y. Yang and W. Gao, "A Bayesian solution to the problem of state estimation in an unknown noise environments," *J. Geodesy*, vol. 80, no. 4, pp. 177–183, 2006.

[21] C. Karlgaard, "Robust adaptive estimation for autonomous rendezvous in elliptical orbit," Ph.D. dissertation, Dept. Aerosp. Ocean Eng., Virginia Polytechnic Institute State University, Blacksburg, VA USA, 2019.

[22] B. Friedland, "Estimating noise variances by using multiple observers," *IEEE Trans. Aerosp. Electron. Syst.*, vol. AES-18, no. 4, pp. 442–448, Jul. 1982.

[23] R. Reynolds, "Robust estimation of covariance matrices," *IEEE Trans. Autom. Control*, vol. 35, no. 9, pp. 1047–1051, Sep. 1990.

[24] J. Dunik, O. Kost, O. Straka, and E. Blasch, "State and measurement noise in positioning and tracking: Covariance matrices estimation and Gaussianity assessment," in *Proc. IEEE/ION Position Location Navigat. Symp.*, 2018, pp. 1326–1335.

[25] Y. Bar-Shalom, "Optimal simultaneous state estimation and parameter identification in linear discrete-time systems," *IEEE Trans. Autom. Control*, vol. AC-17, no. 3, pp. 308–319, Jun. 1972.
[26] J. Burg, D. Luenberger, and D. Wenger, "Estimation of structured covariance matrices," *Proc. IEEE*, vol. 70, no. 9, pp. 963–974, Sep. 1982.
[27] X. Li and Y. Bar-Shalom, "Multiple-model estimation with variable structure," *IEEE Trans. Autom. Control*, vol. 41, no. 4, pp. 478–493, Aug. 1996.
[28] P. Hanlon and P. Maybeck, "Multiple-model adaptive estimation using a residual correlation Kalman filter bank," *IEEE Trans. Aerosp. Electron. Syst.*, vol. 36, no. 2, pp. 393–406, Apr. 2000.
[29] H. Blom and Y. Bar-Shalom, "The interacting multiple model algorithm for systems with Markovian switching coefficients," *IEEE Trans. Autom. Control*, vol. 33, no. 8, pp. 780–783, Aug. 1988.
[30] F. Li, H. Liu, and R. Vaccaro, "Performance analysis for DOA estimation algorithms: Unification, simplification, and observations," *IEEE Trans. Aerosp. Electron. Syst.*, vol. 29, no. 4, pp. 1170–1184, Oct. 1993.
[31] W. Ouyang, Y. Wu, and H. Chen, "INS/Odometer land navigation by accurate measurement modeling and multiple-model adaptive estimation," *IEEE Trans. Aerosp. Electron. Syst.*, vol. 57, no. 1, pp. 245–262, Jan. 2021.
[32] M. Gomaa, O. De Silva, G. Mann, and G. Gosine, "Observability-constrained VINS for MAVs using interacting multiple model algorithm," *IEEE Trans. Aerosp. Electron. Syst.*, vol. 57, no. 3, pp. 1423–1442, Jun. 2021.
[33] L. Xu, X. Li, and Z. Duan, "Hybrid grid multiple-model estimation with application to maneuvering target tracking," *IEEE Trans. Aerosp. Electron. Syst.*, vol. 52, no. 1, pp. 122–136, Jan. 2016.
[34] R. Visina, Y. Bar-Shalom, and P. Willett, "Multiple-model estimators for tracking sharply maneuvering ground targets," *IEEE Trans. Aerosp. Electron. Syst.*, vol. 54, no. 3, pp. 1404–1414, Jun. 2018.
[35] X. Li and Y. Bar-Shalom, "Design of an interacting multiple model algorithm for air traffic control tracking," *IEEE Trans. Control Syst. Technol.*, vol. 1, no. 3, pp. 186–194, Sep. 1993.
[36] Z. Kowalczuk and M. Sankowski, "Soft- and hard-decision multiple-model estimators for air traffic control," *IEEE Trans. Aerosp. Electron. Syst.*, vol. 46, no. 4, pp. 2056–2065, Oct. 2010.
[37] S. Kim, J. Choi, and Y. Kim, "Fault detection and diagnosis of aircraft actuators using fuzzy-tuning IMM filter," *IEEE Trans. Aerosp. Electron. Syst.*, vol. 44, no. 3, pp. 940–952, Jul. 2008.
[38] N. Sadeghzadeh-Nokhodberiz and J. Poshtan, "Distributed interacting multiple filters for fault diagnosis of navigation sensors in a robotic system," *IEEE Trans. Syst., Man, Cybern. Syst.*, vol. 47, no. 7, pp. 1383–1393, Jul. 2017.
[39] M. Mabrouk, G. Ferre, E. Grivel, and N. Deltimple, "Interacting multiple model based detector to compensate power amplifier distortions in cognitive radio," *IEEE Trans. Commun.*, vol. 63, no. 5, pp. 1580–1593, May 2015.
[40] X. Feng, Y. Zhao, Z. Zhao, and Z. Zhou, "Cognitive tracking waveform design based on multiple model interaction and measurement information fusion," *IEEE Access*, vol. 6, pp. 30680–30690, 2018.
[41] X. R. Li and Y. Bar-Shalom, "A recursive multiple model approach to noise identification," *IEEE Trans. Aerosp. Electron. Syst.*, vol. 30, no. 3, pp. 671–684, Jul. 1994.
[42] J. Raquet et al., "Position, navigation, and timing technologies in the 21st century," in *Part D: Position, Navigation, and Timing Using Radio Signals-of-Opportunity*, vol. 2, J. Morton, F. van Diggelen, J. Spilker Jr., and B. Parkinson, Eds. New York, NY, USA: Wiley, 2021, ch. 35–43, pp. 1115–1412.
[43] Z. Kassas, J. Khalife, A. Abdallah, and C. Lee, "I am not afraid of the GPS jammer: Resilient navigation via signals of opportunity in GPS-denied environments," *IEEE Aerosp. Electron. Syst. Mag.*, vol. 37, no. 7, pp. 4–19, Jul. 2022.
[44] N. Souli, P. Kolios, and G. Ellinas, "Online relative positioning of autonomous vehicles using signals of opportunity," *IEEE Trans. Intell. Veh.*, vol. 7, no. 4, pp. 873–885, Dec. 2022.
[45] J. McEllroy, "Navigation using signals of opportunity in the AM transmission band," Master's thesis, Dept. Air Force Air Univ. Air Force Institute of Technology, Wright-Patterson Air Force Base, OH, USA, 2006.
[46] X. Chen, Q. Wei, F. Wang, Z. Jun, S. Wu, and A. Men, "Super-resolution time of arrival estimation for a symbiotic FM radio data system," *IEEE Trans. Broadcast.*, vol. 66, no. 4, pp. 847–856, Dec. 2020.
[47] J. Honda and T. Otsuyama, "Feasibility study on aircraft positioning by using ISDB-T signal delay," *IEEE Antennas Wireless Propag. Lett.*, vol. 15, pp. 1787–1790, 2016.
[48] C. Yang and A. Soloviev, "Mobile positioning with signals of opportunity in urban and urban canyon environments," in *Proc. IEEE/ION Position Location Navigat. Symp.*, 2020, pp. 1043–1059.
[49] J. del Peral-Rosado, J. López-Salcedo, F. Zanier, and G. Seco-Granados, "Position accuracy of joint time-delay and channel estimators in LTE networks," *IEEE Access*, vol. 6, pp. 25185–25199, 2018.
[50] J. Gante, L. Sousa, and G. Falcao, "Dethroning GPS: Low-power accurate 5G positioning systems using machine learning," *IEEE Trans. Emerg. Sel. Topics Circuits Syst.*, vol. 10, no. 2, pp. 240–252, Jun. 2020.
[51] J. Khalife and Z. Kassas, "On the achievability of submeter-accurate UAV navigation with cellular signals exploiting loose network synchronization," *IEEE Trans. Aerosp. Electron. Syst.*, vol. 58, no. 5, pp. 4261–4278, Oct. 2022.
[52] C. Yang, M. Arizabaleta-Diez, P. Weitkemper, and T. Pany, "An experimental analysis of cyclic and reference signals of 4G LTE for TOA estimation and positioning in mobile fading environments," *IEEE Aerosp. Electron. Syst. Mag.*, vol. 37, no. 9, pp. 16–41, Sep. 2022.
[53] Z. Kassas, J. Morales, and J. Khalife, "New-age satellite-based navigation–STAN: Simultaneous tracking and navigation with LEO satellite signals," *Inside GNSS Mag.*, vol. 14, no. 4, pp. 56–65, 2019.
[54] J. Khalife, M. Neinavaie, and Z. Kassas, "The first carrier phase tracking and positioning results with Starlink LEO satellite signals," *IEEE Trans. Aerosp. Electron. Syst.*, vol. 56, no. 2, pp. 1487–1491, Apr. 2022.
[55] N. Jardak and Q. Jault, "The potential of LEO satellite-based opportunistic navigation for high dynamic applications," *Sensors*, vol. 22, no. 7, pp. 2541–2565, 2022.
[56] C. Huang, H. Qin, C. Zhao, and H. Liang, "Phase—Time method: Accurate Doppler measurement for Iridium NEXT signals," *IEEE Trans. Aerosp. Electron. Syst.*, vol. 58, no. 6, pp. 5954–5962, Jun. 2022.
[57] K. Shamaei and Z. Kassas, "LTE receiver design and multipath analysis for navigation in urban environments," *J. Inst. Navigat.*, vol. 65, no. 4, pp. 655–675, Dec. 2018.
[58] K. Shamaei and Z. Kassas, "Receiver design and time of arrival estimation for opportunistic localization with 5G signals," *IEEE Trans. Wireless Commun.*, vol. 20, no. 7, pp. 4716–4731, Jul. 2021.
[59] P. Wang and Y. Morton, "Multipath estimating delay lock loop for LTE signal TOA estimation in indoor and urban environments," *IEEE Trans. Wireless Commun.*, vol. 19, no. 8, pp. 5518–5530, Aug. 2020.
[60] H. Dun, C. Tiberius, and G. Janssen, "Positioning in a multipath channel using OFDM signals with carrier phase tracking," *IEEE Access*, vol. 8, pp. 13011–13028, 2020.
[61] T. Kazaz, G. Janssen, J. Romme, and A. Van der Veen, "Delay estimation for ranging and localization using multiband channel state information," *IEEE Trans. Wireless Commun.*, vol. 21, no. 4, pp. 2591–2607, Apr. 2022.
[62] Z. Kassas, V. Ghadiok, and T. Humphreys, "Adaptive estimation of signals of opportunity," in *Proc. ION GNSS Conf.*, 2014, pp. 1679–1689.
[63] Z. Kassas et al., "Received power characterization of terrestrial cellular signals on high altitude aircraft," in *Proc. IEEE Aerosp. Conf.*, 2022, pp. 1–8.

[64] R. Cassel, D. Scherer, D. Wilburne, J. Hirschauer, and J. Burke, "Impact of improved oscillator stability on LEO-based satellite navigation," in *Proc. ION Int. Tech. Meeting*, 2022, pp. 893–905.
[65] N. Khairallah and Z. Kassas, "An interacting multiple model estimator of LEO satellite clocks for improved positioning," in *Proc. IEEE Veh. Technol. Conf.*, 2022, pp. 1–5.
[66] Y. Bar-Shalom, X. Li, and T. Kirubarajan, *Estimation With Applications to Tracking and Navigation*. New York, NY, USA: Wiley, 2002.
[67] Y. Baram and N. Sandell, "Consistent estimation of finite parameter sets with application to linear system identification," *IEEE Trans. Autom. Control*, vol. AC-23, no. 3, pp. 451–454, Jun. 1978.
[68] A. Thompson, J. Moran, and G. Swenson, *Interferometry and Synthesis in Radio Astronomy*, 2nd ed. Hoboken, NJ, USA: Wiley, 2001.
[69] R. Brown and P. Hwang, *Introduction to Random Signals and Applied Kalman Filtering With Matlab Exercises*, 4th ed. Hoboken, NJ, USA: Wiley, 2012.
[70] J. Khalife and Z. Kassas, "Opportunistic UAV navigation with carrier phase measurements from asynchronous cellular signals," *IEEE Trans. Aerosp. Electron. Syst.*, vol. 56, no. 4, pp. 3285–3301, Aug. 2020.

Joe Khalife (Member, IEEE) received the B.E. degree in electrical engineering, the M.S. degree in computer engineering from Lebanese American University (LAU), Beirut, Lebanon, and the Ph.D. degree in electrical engineering and computer science from the University of California, Irvine, Irvine, CA, USA.

He was a Postdoctoral Fellow with the University of California, Irvine, and member of the Autonomous Systems Perception, Intelligence, and Navigation (ASPIN) Laboratory. From 2012 to 2015, he was a Research Assistant with LAU, and has been a member of the ASPIN Laboratory since 2015. His research interests include opportunistic navigation, autonomous vehicles, and software-defined radio.

Dr. Khalife is a recipient of the 2016 IEEE/ION Position, Location, and Navigation Symposium (PLANS) Best Student Paper Award, 2018 IEEE Walter Fried Award, and 2021 IEEE AESS Robert T. Hill Best Dissertation Award.

Zaher (Zak) M. Kassas (Senior Member, IEEE) received the B.E. degree in electrical engineering from Lebanese American University, Beirut, Lebanon, the M.S. degree in electrical and computer engineering from The Ohio State University, Columbus, OH, USA, the M.S.E. degree in aerospace engineering and the Ph.D. degree in electrical and computer engineering from The University of Texas at Austin, Austin, TX, USA.

He is currently a Professor of Electrical and Computer Engineering with The Ohio State University and the Director of the Autonomous Systems Perception, Intelligence, and Navigation (ASPIN) Laboratory. He is also the Director of the U.S. Department of Transportation Center: Center for Automated Vehicle Research with Multimodal AssurEd Navigation (CARMEN), focusing on navigation resiliency and security of highly automated transportation systems. His research interests include cyber-physical systems, estimation theory, navigation systems, autonomous vehicles, and intelligent transportation systems.

Dr. Kassas was the recipient of the 2018 National Science Foundation (NSF) CAREER Award, 2019 Office of Naval Research (ONR) Young Investigator Program (YIP) Award, 2022 Air Force Office of Scientific Research (AFOSR) YIP Award, 2018 IEEE Walter Fried Award, 2018 Institute of Navigation (ION) Samuel Burka Award, and 2019 ION Col. Thomas Thurlow Award. He is an Associate Editor for IEEE TRANSACTIONS ON AEROSPACE AND ELECTRONIC SYSTEMS and IEEE TRANSACTIONS ON INTELLIGENT TRANSPORTATION SYSTEMS. He is a Distinguished Lecturer of the IEEE Aerospace and Electronic Systems Society.